Pergamon

Geochimica et Cosmochimica Acta, Vol. 65, No. 18, pp. 3005–3025, 2001

0016-7037/01 $20.00 + .00

PII S0016-7037(01)00638-X

Controls on the Cretaceous and Cenozoic evolution of seawater composition, atmospheric CO_2 and climate

K. WALLMANN*
GEOMAR Research Center, Wischhofstraβe 1-3, Kiel, Germany

(*Received October* 9, 2000; *accepted in revised form March* 19, 2001)

Abstract—A new box model for the global carbon-calcium-strontium cycle is developed to simulate the evolution of Cretaceous and Cenozoic seawater and atmosphere. The model accounts for carbon masses in ocean and atmosphere, in carbonate, in particulate organic carbon (POC), and in the mantle. Major processes considered in the model are mantle degassing and hydrothermal fluxes, alteration of oceanic crust, chemical weathering, metamorphism of carbonates, carbonate accumulation, carbonate turnover in subduction zones, and the turnover of POC. Model outputs are partial pressure of CO_2 (pCO_2), seawater pH, concentrations of Ca, Sr, and HCO_3 in seawater as well as the C and Sr isotopic composition of seawater and marine carbonates. A comprehensive review of current fluxes is given to define the flux equations and parameters. Secular trends recorded in marine carbonates are used to constrain the remaining open model parameters. The model includes a new parameterization of silicate weathering considering the contribution of young volcanic deposits. The weathering of these deposits consumes a large fraction of volcanically-released CO_2 and maintains moderate pCO_2 levels during periods of intense mantle degassing and volcanic/tectonic activity. Further negative feed-back is provided by POC burial which is coupled to pCO_2-dependent weathering rates. The model produces high Ca concentrations during the Cretaceous and a strong increase in both pH and carbonate alkalinity during the late Cenozoic. Moreover, it predicts high atmospheric CO_2 and surface temperatures for the mid-Cretaceous and early Cenozoic and low values for the late Cenozoic icehouse world thus suggesting a close coupling between climate and pCO_2. Finally, it demonstrates that the mid-Cretaceous greenhouse was caused by enhanced volcanic/tectonic activity and confirms that the late Cenozoic cooling has been induced by an increase in silicate weatherability caused by enhanced mountain building and erosion.

1. INTRODUCTION

On a million year time scale, the global carbon cycle is mainly controlled through mantle degassing, weathering, sedimentation, as well as diagenesis and metamorphism (Berner et al., 1983). These processes also affect the isotopic and chemical composition of the global ocean. Therefore, marine carbonates that record the composition of ancient seawater can be used to constrain the rates of these processes and the evolution of the global carbon cycle. During the past decades a growing number of box models were developed that simulate the carbon cycle on geological time scales using secular trends in the isotopic composition of marine carbonates (Berner, 1991; Berner, 1994; Caldeira, 1992; Caldeira and Rampino, 1991; Derry and France-Lanord, 1996; François and Goddéris, 1998; Goddéris and François, 1995; 1996; Kump, 1989; Kump and Arthur, 1997; Petsch and Berner, 1998; Richter and Turekian, 1993; Tajika, 1998; Volk, 1989). In these models, the partial pressure of CO_2 in the atmosphere (pCO_2) is usually stabilized by a negative feed-back established by the temperature-dependence of silicate weathering. It is assumed that the global surface temperature is controlled by pCO_2 so that the CO_2 consumption via silicate weathering is enhanced at high pCO_2 levels and vice versa (Berner et al., 1983; Walker et al., 1981). This mechanisms has been questioned by Raymo and Ruddiman (1992) and Edmond et al. (1996) who state that weathering rates are primarily controlled via mechanical erosion and by the lithology of exposed silicate rocks. The importance of these factors is stressed by a recent compilation of field data that reveals physical denudation of continental rocks as a major factor controlling the regional distribution of silicate weathering rates (Gaillardet et al., 1999b). Model studies for the last glacial maximum suggest that the glacial weathering rates were close to the Holocene value (Kump and Alley, 1994; Ludwig et al., 1999) even though the surface temperatures were significantly reduced, thus, also questioning the importance of climate-weathering feed-backs. Moreover, the correlation between pCO_2 and surface temperature is currently under debate. Thus, $\delta^{13}C$ values in sedimentary alkenones indicate that the Miocene climate optimum (14.5–17 My b. p.), the warmest time of the past 35 My, was accompanied by low pCO_2 levels (Flower, 1999; Pagani et al., 1999) and $\delta^{18}O$ values in marine carbonates indicate that tropical surface temperatures and pCO_2 values were decoupled during extended periods of the Phanerozoic (Veizer et al., 2000; Wallmann, 2001).

In this paper, a model of the global carbon cycle is presented that contains new and enhanced formulations of silicate weathering, crust alteration, organic carbon burial, and subduction zone processes. Atmospheric pCO_2, seawater composition (pH, Ca, Sr, HCO_3^-, CO_2, $^{87}Sr/^{86}Sr$, $\delta^{13}C$) and surface temperatures are calculated from the early Cretaceous to the Quaternary to explore the geochemical evolution of ocean and atmosphere, to identify the major controls on seawater composition and pCO_2, and to investigate the role of CO_2 in climate regulation.

* Author to whom correspondence should be addressed (kwallmann@geomar.de).

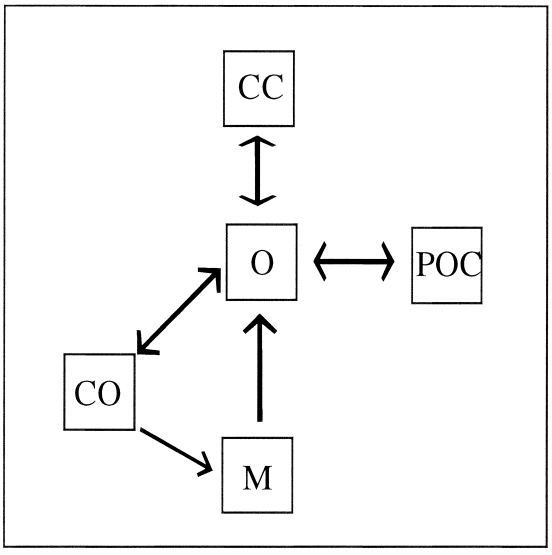

Fig. 1. Set-up of the box model. Carbonate rocks on continental crust (CC), ocean and atmosphere (O), particulate organic carbon (POC), carbonate on oceanic crust (CO) and the earth's mantle (M) are considered as individual reservoirs.

2. DESCRIPTION OF THE MODEL

The model is based on 5 different boxes (Fig. 1). A combined ocean/atmosphere reservoir, that exchanges CO_2, HCO_3, Ca, Sr, ^{87}Sr and ^{13}C with the other boxes, forms the center of the model set-up. Two reservoir are used to balance the amounts of carbonate ($CaCO_3$) on continental and oceanic crust. One more box is devoted to the turnover of particulate organic carbon (POC) and the last box balances the amount of carbon in the mantle. The Quaternary fluxes used in the definition of model fluxes are listed in Table 1 and 2, the equations that define the model fluxes are summarized in Table 3 and the differential equations used for the calculation of reservoir masses, pCO_2 values and seawater concentrations are listed in Table 4.

2.1. Mantle degassing and hydrothermal fluxes

Mantle-CO_2 is released into the exosphere at midocean ridges, volcanic arcs and intraplate volcanoes. Due to the similar solubility of CO_2 and ^3He in ascending magmas and the well constrained ^3He fluxes, the global CO_2 fluxes at spreading centers can be calculated from $CO_2/^3He$ ratios and ^3He fluxes as $(2.2 \pm 0.9) \times 10^{+18}$ mol My^{-1} (Marty and Tolstikhin, 1998). At arc volcanoes, not only mantle-CO_2 but also CO_2 from subducted oceanic plates is released into the atmosphere significantly increasing the $CO_2/^3He$ ratios (Sano and Williams, 1996). Assuming that the mantle component has the same $CO_2/^3He$ ratio as volatiles emitted at midocean ridges, the flux of mantle-CO_2 at arc volcanoes can be estimated as $0.3 - 0.5 \times 10^{+18}$ mol My^{-1} (Marty and Tolstikhin, 1998; Sano and Williams, 1996). Hence, the present-day CO_2 flux from the mantle at active plate boundaries $F_{PB}(p)$ amounts to $(2.6 \pm 1.0) \times 10^{+18}$ mol My^{-1}.

Ca and Sr are leached from basalts and released into the ocean at spreading centers via hydrothermal fluids. The hydrothermal Sr flux can be estimated from marine $^{87}Sr/^{86}Sr$ data and mass balances (Palmer and Edmond, 1989; Richter et al., 1992) as $(1.0 \pm 0.5) \times 10^{+16}$ mol My^{-1} whereas marine Mg balances suggest a hydrothermal Ca flux of approximately $4.8 \times 10^{+18}$ mol My^{-1} (Berner and Berner, 1996).

Following the approach of the BLAG (Berner et al., 1983) and GEOCARB models (Berner, 1991; 1994), a non-dimensional variable (f_{PB}) was constructed (Fig. 2) that describes the change in spreading rates during the Cretaceous and Cenozoic (Larson, 1991a). It is used in the model to calculate the fluxes of CO_2, Ca, and Sr at active plate margins (F_{PB}) through time:

$$F_{PB} = f_{PB} \cdot F_{PB}(q) \quad (1)$$

assuming that the fluxes at midocean ridges and arc volcanoes are proportional to the spreading/subduction rates (Table 3).

The $CO_2/^3He$ ratios of plume-associated intraplate volcanoes are generally close to the values observed at midocean ridges (Marty and Jambon, 1987; Marty and Tolstikhin, 1998; Trull et al., 1993) with an average of $\sim 3 \times 10^{+9}$ (Marty and Tolstikhin, 1998). Assuming that intraplate volcanoes not driven by

Table 1. Quaternary fluxes of CO_2 and HCO_3 (in 10^{+18} mol My^{-1}). Fluxes and mass balances referring to the standard case are given in parenthesis.

Flux	Symbol/Value
Release of mantle-CO_2 at active plate boundaries	$F_{PB}(q) = 2.6 \pm 1.0$ (2.6)
Release of mantle-CO_2 at intra-plate volcanoes	$F_{IP}(q) = 0.6 \pm 0.3$ (0.6)
Uptake of HCO_3 during alteration of oceanic crust	$F_{ALI}(q) = 1.5 - 2.4$ (2.4)
CO_2/HCO_3 turnover during weathering of volcanic rocks	$F^{VO}_{WS}(q) = 3.0$ (3.1)
CO_2/HCO_3 turnover during weathering of other silicate rocks	$F^{S}_{WS}(q) = 8.7$ (8.7)
CO_2 consumption during carbonate weathering	$F_{WC}(q) = 13$ (11.4)
HCO_3 release during carbonate weathering	$2 \times F_{WC}(q)$ (22.8)
CO_2 release during metamorphism of continental carbonates	$F_{MC}(q) = 0.2 - 2$ (0.9)
CO_2 release during carbonate accumulation	$F_{BC}(q) = 18 - 20$ (16.0)
HCO_3 consumption during carbonate accumulation	$2 \times F_{BC}(q)$ (32.0)
CO_2 release from subducted $CaCO_3$	$F_{SC}(q) = 2.3$ (2.5)
CO_2 consumption during POC burial	$F_{BO}(q) = 6$ (5.7)
CO_2 release during POC weathering	$F_{WO}(q) = 6$ (6.2)
CO_2 release from subducted POC	$F_{SO}(q) = 0.2 \pm 0.15$ (0.06)
atmospheric/oceanic CO_2 balance	*−2.25 to + 4.45 (−0.04)*
oceanic HCO_3 balance	*−4.7 to + 0.2 (+0.2)*

Table 2. Quaternary fluxes of Ca (in 10^{+18} mol My^{-1}) and Sr (in 10^{+16} mol My^{-1}). Fluxes and mass balances referring to the standard case are given in parenthesis.

Flux	Symbol/Value
Hydrothermal release of Ca into the ocean	$F^{Ca}_{HY}(q) = 4.8$ (4.8)
Uptake of Ca during alteration of oceanic crust	$F_{ALT}(q) = 1.5 - 2.4$ (2.4)
Ca release during weathering of volcanic rocks	$F^{VO}_{WS,Ca}(q) = 0.75$ (0.77)
Ca release during weathering of other silicate rocks	$F^{S}_{WS,Ca}(q) = 1.52$ (1.53)
Ca release during carbonate weathering	$F_{WC,Ca}(q) = 11.31$ (9.46)
Ca burial during $CaCO_3$ accumulation	$F_{BC}(q) = 18 - 20$ (16.0)
Oceanic Ca balance	*−4.02 to −1.12 (−1.84)*
Hydrothermal release of Sr into the ocean	$F^{Sr}_{HY}(q) = 1.0 \pm 0.5$ (0.5)
Uptake of Sr in authigenic silicate minerals	$F^{Sr}_{A}(q) \approx 0.2 - 2$ (1.6)
Sr release during weathering of volcanic rocks	$F^{VO}_{WS,Sr}(q) = 0.75$ (0.77)
Sr release during weathering of other silicate rocks	$F^{S}_{WS,Sr}(q) = 1.3$ (1.31)
Sr release during carbonate weathering	$F_{WC,Sr}(q) = 0.81$ (0.60)
Sr burial during $CaCO_3$ accumulation	$F_{BC,Sr}(q) = 1.1 - 2.0$ (3.05)
Oceanic Sr balance	*−0.64 to + 3.06 (−1.47)*

mantle plumes have a similar $CO_2/^3He$ ratio as plume associated volcanoes, the present-day ^3He emission at intraplate volcanoes (160 – 240 mol y^{-1}; Allard, 1992) suggests a CO_2 flux of approximately $0.6 \times 10^{+18}$ Mol My^{-1}. The activity of plume-type intraplate volcanism (f_{IP}, Fig. 2) has been reconstructed (Larson, 1991b) and is used here to calculate the CO_2 fluxes at intraplate volcanoes through time.

2.2. Alteration of oceanic crust

The formation of $CaCO_3$ precipitates in upper oceanic crust during low-temperature alteration processes is a major carbon sink ($1.5 – 2.4 \times 10^{+18}$ mol C y^{-1}; Alt and Teagle, 1999) that has to be considered in global carbon balances (Alt and Teagle, 1999; Staudigel et al., 1996; 1990). The dynamics of $CaCO_3$ precipitation are poorly constrained. Therefore, carbon taken up during alteration (F_{ALT}) is separated into a portion precipitated soon after crust formation and a portion bound at a constant rate not affected by tectonic processes:

$$F_{ALT} = F_{ALT}(q) \cdot (r_{ALT} \cdot (f_{PB} - 1) + 1) \quad (2)$$

where $F_{ALT}(q)$ is the current uptake and r_{ALT} defines the fraction (0 – 1) that precipitates rapidly with a rate proportional

Table 3. Fluxes considered in the model.

Flux	Equation
Mantle degassing at active plate margins	$F_{PB} = f_{PB} \cdot F_{PB}(q)$
Mantle degassing at intra-plate volcanoes	$F_{IP} = f_{IP} \cdot F_{IP}(q)$
Uptake of HCO_3 and Ca during alteration of oceanic crust	$F_{ALT} = F_{ALT}(q) \cdot (r_{ALT} \cdot (f_{PB} - 1) + 1)$
Consumption of CO_2 and production of HCO_3 during silicate weathering	$F_{WS} = f_B(CO_2) \cdot (f_A \cdot f_{RUN})^{0.65} \cdot f_{AN} \cdot (F^{VO}_{WS}(q) \cdot (r_{VO} \cdot (f_{VO} - 1) + 1) + f_{ER}^{2/3} \cdot F^{S}_{WS}(q))$
CO_2 consumption during carbonate weathering	$F_{WC} = f_{BB}(CO_2) \cdot f_{LA} \cdot f_A \cdot f_{RUN} \cdot f_{AN} \cdot k_{WC} \cdot CC$
CO_2 release from continental carbonates due to metamorphism	$F_{MC} = k_{MC} \cdot CC$
CO_2 release during carbonate burial	$F_{BC} = k_{BC} \cdot (C_{Ca} \cdot C^2_{HCO_3} - K_C \cdot C_{CO_2})$
CO_2 release from subducted $CaCO_3$	$F_{SC} = r_S \cdot f_{PB} \cdot k_{SC} \cdot CO$
$CaCO_3$ subduction into the mantle	$F_{SM} = (1 - r_S) \cdot f_{PB} \cdot k_{SC} \cdot CO$
CO_2 fixation due to POC burial	$F_{BO} = \left[\frac{F_{WO} + F_{WS} + F_{WC}}{F_{WO}(q) + F_{WS}(q) + F_{WC}(q)}\right] \cdot F_{BO}(q)$
CO_2 release due to POC weathering	$F_{WO} = f^{P}_{ER} \cdot f_A \cdot k_{WO} \cdot POC$
CO_2 release from subducted POC	$F_{SO} = f_{ER} \cdot f_{PB} \cdot k_{SO} \cdot POC$
Hydrothermal release of Ca	$F^{Ca}_{HY} = f_{PB} \cdot F^{Ca}_{HY}(q)$
Release of Ca during silicate weathering	$F^{Ca}_{WS} = f_B(CO_2) \cdot (f_A \cdot f_{RUN})^{0.65} \cdot f_{AN} \cdot (F^{VO}_{WS,Ca}(q) \cdot (r_{VO} \cdot (f_{VO} - 1) + 1) + f^{2/3}_{ER} \cdot F^{S}_{WS,Ca}(q))$
Hydrothermal release of Sr	$F^{Sr}_{HY} = f_{PB} \cdot F^{Sr}_{HY}(q)$
Sr uptake in authigenic silicate minerals	$F^{Sr}_{A} = F^{Sr}_{A}(q)$
Release of Sr during silicate weathering	$F^{Sr}_{WS} = f_B(CO_2) \cdot (f_A \cdot f_{RUN})^{0.65} \cdot f_{AN} \cdot (F^{VO}_{WS,Sr}(q) \cdot (r_{VO} \cdot (f_{VO} - 1) + 1) + f^{2/3}_{ER} \cdot F^{S}_{WS,Sr}(q))$
Release of ^{87}Sr during silicate weathering	$F^{87}_{WS} = f_B(CO_2) \cdot (f_A \cdot f_{RUN})^{0.65} \cdot f_{AN} \cdot (F^{VO}_{WS,Sr}(q) \cdot \Phi^{VO}_{87} \cdot (r_{VO} \cdot (f_{VO} - 1) + 1) + f^{2/3}_{ER} \cdot F^{S}_{WS,Sr}(q) \cdot \Phi^{S}_{87})$
Burial of Sr in marine carbonates	$F^{Sr}_{BC} = D \cdot (Sr/Ca)_{SW} \cdot F_{BC}$

Table 4. Mass balances that define the change in reservoir size (M) with time (dM/dt). The coupled system of first order differential equations given in the table was integrated using finite difference procedures.

Reservoir	Mass balance
CO_2 in ocean and atmosphere	$F_{PB} + F_{IP} + F_{MC} + F_{BC} + F_{SC} + F_{WO} + F_{SO} - F_{WS} - F_{WC} - F_{BO}$
HCO_3 in the ocean	$F_{WS} + 2 \cdot F_{WC} - F_{ALT} - 2 \cdot F_{BC}$
Total C in ocean and atmosphere	$F_{PB} + F_{IP} + F_{MC} + F_{SC} + F_{WC} + F_{WO} + F_{SO} - F_{BC} - F_{ALT} - F_{BO}$
Total ^{13}C in ocean and atmosphere	$\Phi_{13}^{M} \cdot (F_{PB} + F_{IP}) + \Phi_{13}^{C_{in}} \cdot (F_{MC} + F_{SC} + F_{WC}) + \Phi_{13}^{POC_{in}} \cdot (F_{WO} + F_{SO}) - \Phi_{13}^{O} \cdot (F_{BC} + F_{ALT}) - \Phi_{13}^{POC_{out}} \cdot F_{BO}$
Ca in the ocean	$F_{HY}^{Ca} + F_{WS}^{Ca} + 0.83 \cdot F_{WC} - F_{ALT} - F_{BC}$
Sr in the ocean	$F_{HY}^{Sr} + F_{WS}^{Sr} + 6.25 \cdot 10^{-4} \cdot F_{WC} - F_{A}^{Sr} - F_{BC}^{Sr}$
^{87}Sr in the ocean	$\Phi_{87}^{HY} \cdot F_{HY}^{Sr} + F_{WS}^{87} + \Phi_{87}^{WC} \cdot 6.25 \cdot 10^{-4} \cdot F_{WC} - \Phi_{87}^{SW} \cdot (F_{A}^{Sr} + F_{BC}^{Sr})$
Carbonate on continental crust	$f_{BCC} \cdot F_{BC} - F_{MC} - F_{WC}$
Carbonate at the deep-sea floor	$(1 - f_{BCC}) \cdot F_{BC} + F_{ALT} - F_{SC} - F_{SM}$
Particulate organic carbon	$F_{BO} - F_{WO} - F_{SO}$
Carbon in the mantle	$F_{SM} - F_{PB} - F_{IP}$

to the spreading rate f_{PB}. The overall stoichiometry of seafloor weathering can be approximated as (Wallmann, 1999):

$$(Na_2O)_{350}(K_2O)_{9.6}(MgO)_{1900}(CaO)_{2192}(FeO)_{1310}(Fe_2O_3)_{49}(CO_2)_{11}$$
$$(H_2O)_{111}(\text{fresh basalt}) + 46\ Na^+ + 113.8\ K^+ + 377\ Ca^{2+}$$
$$+ 739\ HCO_3^- + 171.5\ O_2 + 1216.9\ H_2O \Rightarrow$$
$$(Na_2O)_{373}(K_2O)_{66.5}(MgO)_{1848}(CaO)_{2569}(FeO)_{620}(Fe_2O_3)_{392}$$
$$(CO_2)_{750}(H_2O)_{1666}(\text{altered crust}) + 52\ Mg^{2+} + 4\ Fe^{2+} + 62.8\ H^+ \quad (3)$$

using the composition of Cretaceous crust strongly altered at low temperatures (Staudigel et al., 1996). These data as well as previous studies (Sansone et al., 1998; Spivack and Staudigel, 1994) show that the formation of $CaCO_3$ precipitates in oceanic crust is not accompanied by a significant production of CO_2 or acidity because the acid released during carbonate precipitation is consumed in other seafloor weathering processes. In the model, carbonate formation during alteration of oceanic crust is, thus, only a sink for HCO_3 whereas sedimentation of carbonate acts both as HCO_3 sink and CO_2 source. The major fraction of Ca fixed in carbonate precipitates is taken up from seawater (Alt and Teagle, 1999). Therefore, removal of seawater Ca via alteration of oceanic crust corresponds approximately to HCO_3 fixation. Sr is bound in smectites and other clay minerals formed during seafloor alteration (Staudigel et al., 1995; 1996) and reverse weathering processes in marine sediments (Michalopoulos and Aller, 1995). The rates of these reactions are determined by modelling of seawater Sr and Sr/Ca ratios.

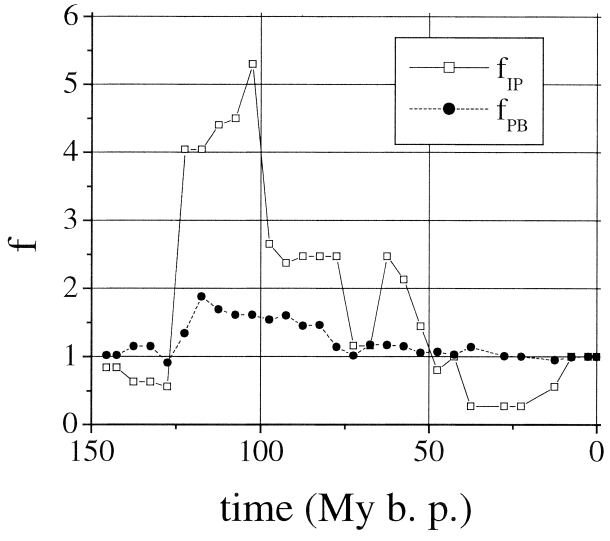

Fig. 2. Changes in spreading/subduction rates (f_{PB}) and in the activity of intraplate volcanism (f_{IP}) through time (Larson; 1991a; b). All data were normalized to the present values to calculate the non-dimensional variables f_{PB} and f_{IP}.

2.3. Silicate weathering

Silicate weathering is of prime importance in the modeling of the global carbon cycle because it converts large quantities of CO_2 into HCO_3 and produces dissolved Ca and Sr. The current weathering rates of volcanic deposits and other silicate rocks were recently determined by Gaillardet et al. (1999b). As the silicate weathering rates during the last glacial maximum are close to the Holocene values (Gibbs and Kump, 1994; Ludwig et al., 1999), these data can be used to define the average Quaternary fluxes applied in the modeling (Tables 1 and 2).

Weathering rates depend on climate (runoff and temperature), abundance and type of terrestrial vegetation, physical erosion rates, and lithology of the drainage area (Berner and Berner, 1996; Gaillardet et al., 1999b). In the model, the weathering fluxes (F_{WS}) were calculated using the following equation:

$$F_{WS} = f_B(CO_2) \cdot (f_A \cdot f_{RUN})^{0.65} \cdot f_{AN} \cdot (F_{WS}^{VO}(q) \cdot (r_{VO} \cdot (f_{VO} - 1) + 1) + f_{ER}^{2/3} \cdot F_{WS}^{S}(q)) \quad (4)$$

The variable $f_B(CO_2)$ depends on pCO_2 and defines a strong negative feed-back effectively stabilizing the pCO_2 level (Berner, 1991; 1994). It was taken from the GEOCARB II model (Berner, 1994) and considers the impact of surface

temperature, pCO_2 and runoff on the weathering kinetics where runoff depends in surface temperature and the surface temperature is in turn controlled via pCO_2 and changing solar luminosity (Eqn. 26). Improved estimates for the temperature-dependence of global runoff and the sensitivity of surface temperature with respect to solar luminosity and pCO_2 (Kothavala et al., 1999; 2000) were included in the parameterization of $f_B(CO_2)$ following the approach used in the new GEOCARB III model (Berner and Kothavala, 2001). The non-dimensional variable f_{RUN} gives the change in runoff due to changes in paleogeography (Otto-Bliesner, 1995). It is multiplied with the change in land area (f_A; Ronov, 1994) to convert runoff, given in terms of volume of water per area per time, into discharge in terms of volume of water per time. The non-linear dependence of silicate weathering on discharge (f_{RUN} f_A) is considered using the exponent 0.65 (Berner, 1994). The enhancement of weathering caused by the rise of angiosperms during the Cretaceous is expresses by the non-dimensional parameter f_{AN} (Berner, 1994).

In contrast to the previous modeling, silicate rocks were separated into two different types associated with different variables as defined in the last term of Eqn. 4 where $F^{VO}_{WS}(q)$ and $F^{S}_{WS}(q)$ are Quaternary rates caused by the weathering of young volcanic deposits and other silicate rocks, respectively (Tables 1 and 2). Young volcanic deposits contain glass and very reactive silicate minerals such as olivine and plagioclase that are completely weathered within less than 20 000 yr under favorable climatic conditions (Louvat and Allègre, 1997; Vitousek et al., 1997). Weathering rates may be further accelerated by the high volatile contents of groundwaters from around volcanoes that promote dissolution reactions (Aiuppa et al., 2000). Currently, most subaerial deposits of volcanic rocks and ashes are produced in subduction zones. Here, the proportion of ashes and other clastic material is very high due to the enhanced volatile contents of the ascending magmas. The resulting tephra deposits are easily eroded and exposed to water so that weathering can proceed rapidly under humid and warm conditions. With respect to the million year time scale of the model, a large fraction of tephra is weathered soon after deposition so that it is reasonable to relate the weathering of volcanic deposits to the production rate of volcanics. The magma production in volcanic arcs is triggered by convection in the mantle wedge overlying the subducted slap and by fluids expelled from the slap. Both, convection and fluid input are driven by subduction of the incoming oceanic plate. The global rates of subduction (Engebretson et al., 1992) closely correspond to global spreading rates (Larson, 1991b). Therefore, enhanced spreading accelerates subduction and magma production in volcanic arcs. A non-dimensional variable (f_{VO}) that defines the change in total volcanic activity caused by spreading/subduction and ascending mantle plumes:

$$f_{VO} = \frac{F_{PB} + F_{IP}}{F_{PB}(q) + F_{IP}(q)} \quad (5)$$

is thus used to scale the weathering rates of volcanic deposits (see also section 2.1 and Fig. 2). Moreover, weathering of volcanic deposits is separated into a component coupled to production and an other component that is constant through time (see also Eqn. 2 in section 2.2). The fraction coupled to production is defined by the parameter r_{VO} and may be regarded as the reactive or exposed portion.

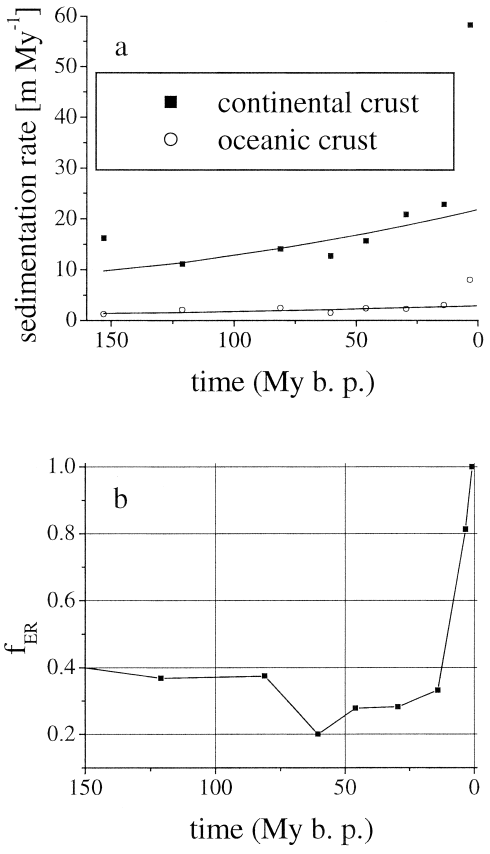

Fig. 3. Sedimentation and erosion rates. (a) Apparent sedimentation rates of terrigenous matter on continental and oceanic crust. The data were determined by Ronov (1993), translated and recompiled by W. W. Hay (pers. commun.) and re-evaluated using the time scale of Harland et al. (1990). The lines represent model curves fitted to the data. (b) Non-dimensional erosion rates (f_{ER}) derived from reconstructed accumulation rates of terrigenous sediments.

The weathering of sedimentary and crystalline rocks is tightly coupled to physical erosion (Gaillardet et al., 1999a). Erosion rates are reflected in the accumulation rates of terrigenous sediments which were reconstructed by Ronov (1993). Figure 3a shows the apparent sedimentation rate of terrigenous matter based on the fraction preserved to date in terms of volume of sediment per area per unit time. The area refers only to that fraction of the depositional area that has been conserved to date to minimize the effect of subduction on the preservation of sediments deposited on oceanic crust. The decay of sedimentary rocks via erosion and metamorphism follows first order kinetics (Veizer and Jansen, 1979). A non-linear fit routine was applied to the sedimentation rates plotted in Figure 3a to determine the decay constants as $(5.35 \pm 1.26) \times 10^{-3}$ My^{-1} and $(4.84 \pm 2.32) \times 10^{-3}$ My^{-1} for sediments deposited on continental and oceanic crust, respectively. The youngest period considered in the data (Pliocene) was omitted in the fitting procedure because this period is influenced by glacial conditions that significantly enhanced erosion. The initial sedimentation rates ($y(0)$) were calculated using the equation:

$$y(0) = y(t) \cdot e^{+b \cdot t} \quad (6)$$

where $y(t)$ are the apparent sedimentation rates plotted in Figure 3a and b is the first order decay constant. The $y(0)$ values were multiplied with the total areas available for sedimentation at the time of deposition (Ronov, 1993) to obtain sedimentation rates in unit volume per unit time. These rates were summed to obtain global accumulation rates and finally normalized to the Quaternary value assuming that the Quaternary sedimentation rate was 23% higher than the Pliocene value (Hay, 1994) to obtain the non-dimensional variable f_{ER} plotted in Figure 3b. The data show that the deposition of terrigenous sediments and hence the erosion of silicate rocks was extremely severe during the Quaternary and Pliocene due to intensified glaciation as previously demonstrated by Hay (1994). Goddéris and François (1995) and Berner and Kothavala (2001) also used erosion rates as a forcing to silicate weathering. The data of Gaillardet et al. (1999a; b) imply that the rate of silicate weathering is proportional to $f_{ER}^{2/3}$ (Berner and Kothavala, 2001).

2.4. Carbonate weathering

The weathering of carbonate rocks is a major CO_2 sink and HCO_3 source in the global carbon cycle. Currently, $12.3 \times 10^{+18}$ mol CO_2 My^{-1} are consumed by the turnover of continental carbonates (Gaillardet et al., 1999b). Under glacial conditions, this weathering rate is probably enhanced by 30% (Ludwig et al., 1999) due to the exposure of shelf carbonates so that the average Quaternary CO_2 consumption rate amounts to approximately $13 \times 10^{+18}$ mol CO_2 My^{-1}. The rate of carbonate weathering is given as (Berner, 1994):

$$F_{WC} = f_{BB}(CO_2) \cdot f_{LA} \cdot f_A \cdot f_{RUN} \cdot f_{AN} \cdot k_{WC} \cdot CC \quad (7)$$

where $f_{BB}(CO_2)$ depends on pCO_2, f_{LA} represents the exposed area of carbonate rocks and the other three variables (f_A, f_{RUN}, f_{AN}) are defined as above (Eqn. 4). Enhanced formulations for the temperature—pCO_2 and runoff-temperature relationships used in the new GEOCARB III model (Berner and Kothavala, 2001) are considered in the calculation of $f_{BB}(CO_2)$. The CO_2 consumption during carbonate weathering (F_{WC}) depends additionally on the amount of carbonate on continental crust (CC, currently $\sim 4 \times 10^{+21}$ mol; Berner, 1982; Hay et al., 1988) thus following first order kinetics with a kinetic constant ($k_{WC} = 3 \times 10^{-3}$ My^{-1}) defined as ratio between the Quaternary flux and reservoir size. The other fluxes (Ca, HCO_3, Sr) are calculated from the CO_2 turnover (F_{WC}) using appropriate stoichiometric ratios (Gaillardet et al., 1999b; Tables 1–4).

2.5. Metamorphism of carbonates on continental crust

Metamorphic decomposition of carbonates produces a significant amount of CO_2 that can be transported to the surface with circulating groundwater (Kerrick and Caldeira, 1998). The present-day global metamorphic CO_2 flux is in the order of 10^{+18} Mol My^{-1} (Kerrick et al., 1995). It changed considerably in the past reaching high values ($\sim 3 \times 10^{+18}$ Mol My^{-1}) during the Early Eocene warmth (55 – 60 My) due to intense hydrothermal activity in the Cordilleran orogen (Kerrick and Caldeira, 1998). In the present study, the metamorphic CO_2 flux (F_{MC}) was assumed to follow first order kinetics with respect to the carbonate mass on continental crust. Considering a metamorphic flux of $(0.5 - 2) \times 10^{+18}$ mol CO_2 My^{-1}, the kinetic constant k_{MC} falls in the range of 1 to 5×10^{-4} My^{-1}.

2.6. Carbonate accumulation

Carbonate accumulates at a rate 18 to $20 \times 10^{+18}$ mol My^{-1} during the Quaternary (Hay and Southam, 1977; Holland, 1984; Opdyke and Walker, 1992). Over the model period, the deposition of Mg-bearing carbonates can be neglected because the accumulation is clearly dominated by biogenic $CaCO_3$. Thus, the overall reaction stoichiometry is simply:

$$Ca^{2+} + 2\,HCO_3^- = CaCO_3(s) + CO_2 + H_2O \quad (8)$$

Carbonate accumulation is limited by the saturation state of the ocean with respect to calcite. Hence, high inputs of HCO_3 and Ca enhance the $CaCO_3$ deposition and vice versa, thus, establishing a negative feed-back that effectively buffers the carbonate alkalinity and the pH of seawater (Broecker and Peng, 1982). In the model, the total carbonate accumulation on continental and oceanic crust (F_{BC}) is defined as:

$$F_{BC} = k_{BC} \cdot (C_{Ca} \cdot C_{HCO_3}^2 - K_C \cdot C_{CO_2}) \quad (9)$$

where k_{BC} is a kinetic constant, C_{Ca}, C_{HCO_3}, and C_{CO_2} are concentrations of Ca, HCO_3, and CO_2 in seawater and K_C is the calcite solubility product that defines the concentrations at thermodynamic equilibrium (eq):

$$K_C = \left(\frac{C_{Ca} \cdot C_{HCO_3}^2}{C_{CO_2}} \right)_{eq} \quad (10)$$

A value of 3×10^{-3} Mol^2 dm^{-6} is assigned to K_C corresponding to the solubility of calcite at 400 bar, 2°C and a salinity of 35 ‰ (Millero, 1995). The kinetic constant k_{BC} is set to $1 \times 10^{+9}$ mol^{-2} dm^{+9} My^{-1}. Model runs showed that the concentration ratio $C_{Ca}\,C_{HCO_3}^2/C_{CO_2}$ was kept in a range of 2.0 to 2.5×10^{-3} Mol^2 dm^{-6} through this parameterization, thus, ascertaining similar conditions as currently observed in average seawater (Archer, 1996a). Salinity and temperature changes have an opposite effect on calcite solubility so that the net effect is rather small and neglected in the model. A similar formulation of calcite accumulation was previously used in the BLAG model (Berner et al., 1983).

Seawater concentrations (C_{Ca}, C_{HCO_3}, and C_{CO_2}) were calculated from the masses of Ca, HCO_3 and CO_2 in the ocean/atmosphere box that were determined for each time step using the mass balances listed in Table 4. Masses were converted into concentrations using a constant seawater volume considering also that a significant portion of CO_2 resides in the atmosphere (section 2.11.).

Total $CaCO_3$ accumulation was further divided into fractions deposited on continental and oceanic crust:

$$F_{BC} = f_{BCC} \cdot F_{BC} + (1 - f_{BCC}) \cdot F_{BC} \quad (11)$$

where the non-dimensional variable f_{BCC} defines the portion of $CaCO_3$ accumulated on the continental shelf and slope. The change of this variable through time is illustrated in Figure 4. It was calculated using data of Hay (1998) who evaluated the apparent accumulation rates reported by Ronov (1993) to de-

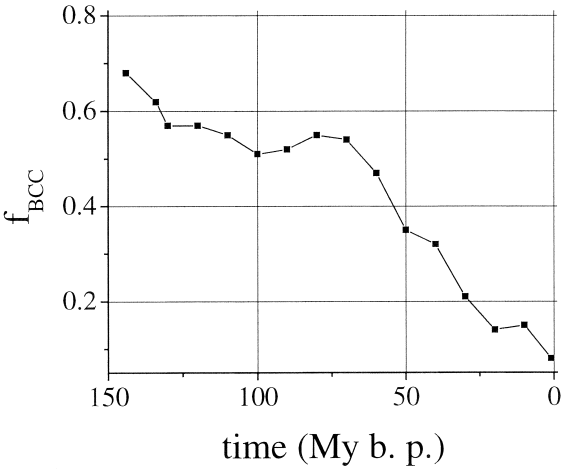

Fig. 4. Fraction of carbonate accumulated on continental crust (f_{BCC}; Hay, 1998).

termine the total carbonate accumulation and the carbonate accumulation on continental crust. The fraction deposited on continental crust decreased drastically during the Cenozoic due to the marine regression, the radiation of plankton with carbonate shells or a change in the saturation state of the deep ocean caused by increasing inputs of carbonate alkalinity (Hay and Southam, 1975; Opdyke and Wilkinson, 1988).

The Sr/Ca ratio in marine carbonates $(Sr/Ca)_C$ depends on the Sr/Ca ratio in seawater $(Sr/Ca)_{SW}$. Thus, Sr burial due to carbonate accumulation is formulated as:

$$F_{BC}^{Sr} = D \cdot (Sr/Ca)_{SW} \cdot F_{BC} \quad (12)$$

where D is a distribution coefficient defined as $D = (Sr/Ca)_C/(Sr/Ca)_{SW}$. The Sr content of seawater is stabilized through this process because the Sr burial is enhanced at high Sr levels and vice versa. D has a constant value of 0.1 calculated from the recent Sr/Ca ratios in seawater and deep-sea carbonates (Renard, 1986). The Sr/Ca ratio in shelf carbonates is reduced to a similar value upon early diagenesis so that Eqn. 12 can be used to simulate Sr accumulation in both deep-sea and shelf carbonates.

2.7. $CaCO_3$ turnover in subduction zones

Carbonate entering subduction zones with the incoming oceanic plates is partly recycled into the atmosphere as volcanic CO_2 and partly subducted into the mantle. The carbonate input is composed of $CaCO_3$ precipitated within the oceanic crust ($1.5 - 2.4 \times 10^{+18}$ mol My^{-1}; Alt and Teagle, 1999) and $CaCO_3$ deposited as biogenic sediment on the deep-sea floor ($2.2 \times 10^{+18}$ mol My^{-1}; Rea and Ruff, 1996). The rate of pelagic $CaCO_3$ accumulation ($10 - 11 \times 10^{+18}$ mol My^{-1}) is currently much higher than the rate of $CaCO_3$ subduction because a large $CaCO_3$ fraction accumulates in the Atlantic which is surrounded by passive continental margins (Archer, 1996b). This imbalance in the sedimentary $CaCO_3$ cycle causes a strong increase in the mass of pelagic carbonate during the Cenozoic. The analysis of volcanic gases ($\delta^{13}C$, ^3He) sampled at arc volcanoes indicates a considerable reflux of CO_2 from subducted carbonates ($\approx 2.3 \times 10^{+18}$ mol My^{-1}; Sano and Williams, 1996) whereas high-pressure experiments and modelling of metamorphism suggest that most of the incoming $CaCO_3$ is subducted deeply into the mantle (Molina and Poli, 2000).

In the model, the CO_2 emission at arc volcanoes due to recycling of subducted carbonates (F_{SC}) is defined as:

$$F_{SC} = r_S \cdot f_{PB} \cdot k_{SC} \cdot CO \quad (13)$$

where r_S is the recycling efficiency of carbonate at subduction zones and f_{PB} is the spreading/subduction variable (Fig. 2). The kinetic constant ($k_{SC} = 0.01$ My^{-1}) is determined as ratio between the Quaternary $CaCO_3$ accumulation rate and the current reservoir size ($1.2 \times 10^{+21}$ mol; Hay et al., 1988; Staudigel et al., 1996). The amount of $CaCO_3$ deposited in and on oceanic crust (CO) is calculated for each time step using the appropriate differential equation (Table 4). Inorganic carbon in oceanic crust that originates directly from the mantle is not considered in the model assuming that the mantle-CO_2 bound in oceanic crust is completely subducted back into the mantle. By this approach the definition of an additional reservoir (oceanic crust) is avoided. The deep subduction of $CaCO_3$ produced via precipitation of marine HCO_3 is considered in the model (F_{SM}, Table 3) because it affects the carbon mass in the mantle (Table 4). It is defined using the fraction of incoming carbon that is not recycled into the atmosphere ($1 - r_S$).

2.8. Turnover of particulate organic carbon

Weathering of POC can be regarded as a major CO_2 source but the rate of this process is only poorly constrained ($2.5–22 \times 10^{+18}$ mol My^{-1}; Kramer, 1994). Due to the rapid oxidation of POC with atmospheric oxygen, the weathering rate is mainly limited by the exposure of POC-bearing rocks to the atmosphere (Berner and Berner, 1996) which is in turn related to the erosion rate of terrigenous matter (f_{ER}). Moreover, the amount of POC and the exposed land area (f_A) affect the weathering rate resulting in the following formulation:

$$F_{WO} = f_{ER}^{p} \cdot f_A \cdot k_{WO} \cdot POC \quad (14)$$

where the kinetic constant ($k_{WO} = 2 - 18 \times 10^{-3}$ My^{-1}) is defined as the ratio of the Quaternary flux and POC mass ($1.25 \times 10^{+21}$ mol; Berner, 1982) and the exponent p is currently unknown. Metamorphism of POC on continental crust is not considered explicitly in the model but summarized under the POC weathering flux.

Burial of POC is an important CO_2 sink. The Holocene accumulation rate ($13 \times 10^{+18}$ mol My^{-1}; Hedges and Keil, 1995) is higher than the Quaternary average, estimated here as $6 \times 10^{+18}$ mol My^{-1}, due to the exposure and erosion of continental shelves during glacial low-stands of sea-level (Broecker, 1982). The accumulation is limited by the supply of nutrients to the ocean which is mainly accomplished by phosphate dissolved in river waters and absorbed on riverine particles. Phosphate is mobilized during weathering of POC and phosphate-bearing minerals. Therefore, the riverine phosphate flux is proportional to chemical weathering (Föllmi, 1995; 1996) so that CO_2 consumption due to POC burial (F_{BO}) is defined as:

$$F_{BO} = \left(\frac{F_{WO} + F_{WS} + F_{WC}}{F_{WO}(q) + F_{WS}(q) + F_{WC}(q)} \right) \cdot F_{BO}(q) \quad (15)$$

where (q) indicates Quaternary fluxes.

POC turnover in subduction zones is not well known. Most POC entering the deep-sea trenches is bound in terrigenous sediments that originate from the adjacent continental margins. A major but largely unknown POC fraction is neither subducted nor recycled into ocean and atmosphere but accumulated within the subduction zone via accretion and/or underplating (Von Huene and Scholl, 1991). The current POC input into subduction zones ($0.54 \times 10^{+18}$ mol My^{-1}) can be estimated from the input flux of terrigenous and biogenic sediments ($1 \times 10^{+21}$ g $My^{-1}$and $2 \times 10^{+20}$ g My^{-1}; Plank and Langmuir, 1998) and the average POC contents of these sediments (0.6 wt-% and 0.25 wt-%; Emerson and Hedges, 1988). Within the subduction zone, POC is degraded into dissolved CO_2 and CH_4 via diagenesis and metamorphism. The evaluation of fluid data from cold vents and mud volcanoes indicates that the steady-state carbon release via fluid venting in the fore-arc area of subduction zones is small ($0.04 \pm 0.02 \times 10^{+18}$ mol My^{-1}; Wallmann, 1999) due to the efficient carbon fixation in authigenic $CaCO_3$ and gas hydrates. In contrast, a considerable fraction of the incoming organic carbon ($0.1–0.5 \times 10^{+18}$ mol My^{-1}) may be recycled back into the atmosphere as CO_2 both at arc volcanoes (Sano and Williams, 1996) and in the back-arc area (Seward and Kerrick, 1996). In the model, the CO_2 flux from diagenetic and metamorphic degradation of POC in subduction zones depends on the total amount of POC and the rates of subduction (f_{PB}) and erosion (f_{ER}) as:

$$F_{SO} = f_{ER} \cdot f_{PB} \cdot k_{SO} \cdot \mathrm{POC} \quad (16)$$

where the value of the kinetic constant ($k_{SO} = (2 \pm 1.5) \times 10^{-4}$ My^{-1}) is again determined from the ratio of Quaternary flux to POC mass.

The formulation of POC fluxes used in the model (Eqn. 15–17) is highly simplifying because the main focus of the model is on the inorganic carbon cycle. More evolved parameterizations were recently developed to simulate not only pCO_2 changes but also the evolution of the partial pressures of oxygen in the atmosphere (Petsch and Berner, 1998; Van Cappellen and Ingall, 1996). The net accumulation of POC is controlled mainly via silicate and carbonate weathering. As weathering is linked to temperature and pCO_2, this parameterization defines a negative feed-back on pCO_2.

2.9. Stable carbon isotopes

The isotopic composition of inorganic carbon dissolved in seawater as recorded in marine carbonates (Veizer et al., 1999; Veizer and Hoefs, 1976) can be used to constrain the turnover of organic carbon because POC formation is associated with a large isotopic fractionation (Hayes et al., 1999). On the timescale of the model, the isotopic exchange reactions between HCO_3, atmospheric and dissolved CO_2 are sufficiently fast to simulate only the isotopic composition of total carbon in the ocean/atmosphere box using the appropriate mass balances (Table 4). The mole fraction of ^{13}C (Φ_{13}) defined as:

$$\Phi_{13} = \frac{^{13}C}{^{12}C + ^{13}C} = \frac{^{13}C}{C} = \frac{1000 + \delta^{13}C}{89990 + \delta^{13}C} \quad (17)$$

is used to calculate ^{13}C fluxes (F_i^{13})

$$F_i^{13} = \Phi_{13} \cdot F_i \quad (18)$$

where $\delta^{13}C$ values refer to the PDB scale (Hoefs, 1997) and F_i is the corresponding carbon flux. The input fluxes of carbon into ocean and atmosphere have a constant Φ_{13} or $\delta^{13}C$ value over the considered period. These include the release of CO_2 from the mantle at active plate boundaries (F_{PB}) and intraplate volcanoes (F_{IP}) with an average mole fraction (Φ_{13}^{M}) of 0.01106 corresponding to a $\delta^{13}C$ value of -5 ‰ (Hoefs, 1997) as well as the carbon fluxes caused by metamorphism and weathering of continental carbonates (F_{MC} and F_{WC}) and the subduction of pelagic carbonates (F_{SC}) which are multiplied with a constant mol fraction ($\Phi_{13}^{C_{in}} = 0.01113$) derived from the average isotopic composition of Phanerozoic carbonates ($+2$ ‰; Veizer et al., 1999). Only, the isotopic composition of CO_2 released during weathering and subduction of POC (F_{WO} and F_{SO}) changed during the late Cenozoic due to the recycling of freshly deposited POC with enhanced ^{13}C contents (Hayes et al., 1999). In the model, a constant $\delta^{13}C$ value of -27.5 ‰ is used for the Cretaceous and early Tertiary followed by a linear increase from -27.5 ‰ to -24.0 ‰. over the last 25 My (Hayes et al., 1999).

Output fluxes caused by the burial of carbonates (F_{BC}) and POC (F_{BO}) as well as by alteration of oceanic crust (F_{ALT}) are related to the time-dependent isotopic composition of carbon in ocean and atmosphere (Φ_{13}^{O}). The small isotopic difference between total dissolved inorganic carbon and marine carbonates (≈1 ‰; Romanek et al., 1992) is neglected in the model so that ^{13}C fixation due to carbonate burial and crust alteration results as:

$$F_{BC}^{13} = \Phi_{13}^{O} \cdot F_{BC} \text{ and } F_{ALT}^{13} = \Phi_{13}^{O} \cdot F_{ALT} \quad (19)$$

where Φ_{13}^{O} is calculated for each time step using the changing masses of total carbon and ^{13}C in ocean and atmosphere. This formulation induces a buffering of marine $\delta^{13}C$ values because ^{13}C removal is enhance at high Φ_{13}^{O} values and vice versa.

The formation and burial of POC is associated with a strong isotopic fractionation that has changed significantly during geological history due to changing pCO_2 levels and radiation of new carbon-fixing species in the terrestrial and marine environments (Hayes et al., 1999). The time-dependent fractionation factor α_{POC} defined as

$$\alpha_{POC} = \frac{(^{13}C/^{12}C)_{POC}}{(^{13}C/^{12}C)_{O}} \approx \frac{(^{13}C/^{12}C)_{POC}}{(^{13}C/^{12}C)_{CaCO_3}} \quad (20)$$

was determined using a recent compilation of $\delta^{13}C$ values measured in marine carbonates and POC (Hayes et al., 1999) which revealed a rather constant fractionation during the Cretaceous and a significant decrease in α_{POC} during the late Cenozoic. These values were then used to determine the isotopic composition of buried POC ($\Phi_{13}^{POC_{out}}$) that depends also on Φ_{13}^{O}:

$$\Phi_{13}^{POC_{out}} = \frac{\alpha_{POC} \cdot \Phi_{13}^{O}}{\alpha_{POC} \cdot \Phi_{13}^{O} + 1 - \Phi_{13}^{O}} \quad (21)$$

This time-dependent mole fraction was in turn multiplied with the POC burial flux (F_{BO}) to calculate the ^{13}C removal due to POC burial (F^{13}_{BO}).

2.10. Strontium isotopes

The $^{87}Sr/^{86}Sr$ ratio in seawater is homogenous throughout the ocean and shows a well defined secular trend in marine carbonates (Veizer et al., 1999). It mainly reflects the intensity of silicate weathering and seafloor spreading releasing radiogenic Sr with high $^{87}Sr/^{86}Sr$ ratios and basaltic Sr with low ratios into the ocean, respectively. An isotopic signature has to be assigned to each of the Sr fluxes considered in the model (Table 3) to calculate the isotopic composition of marine Sr. The mol fraction of ^{87}Sr (Φ_{87}) used in the model is related to the commonly used $^{87}Sr/^{86}Sr$ ratio (R_{87}) as:

$$\Phi_{87} = \frac{^{87}Sr}{^{84}Sr + ^{86}Sr + ^{87}Sr + ^{88}Sr} = \frac{^{87}Sr}{Sr} = \frac{R_{87}}{9.43 + R_{87}} \qquad (22)$$

where the constant 9.43 is defined by the abundance of the different Sr isotopes (Hoefs, 1997) considering that the variation in the isotopic ratio is caused mainly by variable ^{87}Sr contents.

In the model, each Sr flux is multiplied with an appropriate ^{87}Sr mol fraction to calculate the corresponding ^{87}Sr flux (Tables 3 and 4). The isotopic ratio of Sr released from weathering silicates ranges from 0.705 for young volcanic drainage areas to 0.735 for old crystalline basement areas (Gaillardet et al., 1999b). In general, $^{87}Sr/^{86}Sr$ ratios increase with age and initial content of the ^{87}Rb parent nuclide. The situation is complicated by the fact that Rb-bearing and thus ^{87}Sr-rich minerals are relatively inert so that partial weathering of old and highly radiogenic crystalline rocks tends to give dissolved isotope ratios much lower than those in the parent rocks (Edmond, 1992). The average isotopic composition of Sr released from sedimentary and crystalline silicate rocks can be estimated as $R^S_{87} = 0.718$ using an isotopic mass balance based on the Sr isotopic composition of average river water ($R_{87} = 0.7117$; Palmer and Edmond, 1989), weathering volcanic deposits ($R^{VO}_{87} = 0.705$; Gaillardet et al., 1999b), carbonates ($R^{WC}_{87} = 0.708$; Gaillardet et al., 1999b) and the relative contributions of individual weathering fluxes to the total riverine Sr flux (Gaillardet et al., 1999b). The present $^{87}Sr/^{86}Sr$ ratio of river water is affected by highly radiogenic Sr released from the central Himalayas (Edmond, 1992). Excluding the Himalayan rivers, the current $^{87}Sr/^{86}Sr$ ratio of average river water would correspond to only 0.7109 (François and Goddéris, 1998) and the $^{87}Sr/^{86}Sr$ ratio in non-volcanic silicate rocks (R^S_{87}) would reduce to 0.716. Recent isotope models indicate that the impact of the Himalayan orogeny on the marine $^{87}Sr/^{86}Sr$ started at 40 My b. p. (François and Goddéris, 1998; Goddéris and François, 1996). Thus, I assumed a constant $R^S_{87} = 0.716$ for 145 to 40 My b. p. and a linear increase in R^S_{87} over the last 40 My b. p. to the recent value of $R^S_{87} = 0.718$. Hydrothermal Sr leached from basalts at the seafloor is isotopically light with an average ratio of $R^{HY}_{87} = 0.703$ (Teagle et al., 1996). The isotopic composition of Sr removed from the ocean via carbonate burial and alteration of oceanic crust corresponds to the isotopic composition of Sr in the ocean (Φ^{SW}_{87}) which is calculated for each time step using the Sr and ^{87}Sr mass balances listed in Table 4.

2.11. Calculation of pCO_2 values and other model variables

Masses of CO_2, HCO_3, Ca, Sr, ^{13}C, and ^{87}Sr in ocean and atmosphere, masses of $CaCO_3$ deposited on continental and oceanic crust, the sedimentary mass of POC and the mass of carbon in the mantle were calculated for each time step by numerical integration of the partly coupled system of first order differential equation defined in Table 4 using the flux definitions listed in Table 3. Masses of HCO_3, Ca and Sr in the ocean were converted into seawater concentrations using a constant seawater volume of $1.37 \times 10^{+21}$ dm^3 (Broecker and Peng, 1982). The CO_2 mass was distributed between ocean and atmosphere assuming equilibrium conditions:

$$C(CO_2) = \alpha_H \cdot pCO_2 \qquad (23)$$

where $C(CO_2)$ is concentration of CO_2 in the ocean, pCO_2 is partial pressure of CO_2 in the atmosphere and α_H is the Henry constant. The mass of CO_2 in the atmosphere ($M(CO_2)$ in 10^{+18} mol) is related to the partial pressure (pCO_2 in atm) as $M(CO_2) = 1.8 \times 10^{+20} \times pCO_2$ (Siegenthaler and Sarmiento, 1993) whereas the mass of CO_2 in the ocean is calculated from the concentration and the seawater volume. The Henry constant depends on temperature, salinity and pressure. A constant value of 0.04 mol dm^{-3} atm^{-1} (valid for 15°C, 35‰; 1 atm; Millero, 1995) was used in the model. Sensitivity tests showed that the value of α_H had no significant effect on the calculated pCO_2 because the atmospheric CO_2 level is not controlled via air/sea exchange but by the interaction with other reservoirs (continental rocks, sediments, mantle) on the time-scale of the model. Calculated pCO_2 values were normalized to the Quaternary value (230 μatm; Petit et al., 1999) and expressed as non-dimensional RCO_2 values (Berner, 1991). pH values were calculated from CO_2 and HCO_3 concentrations in seawater using the equation:

$$pH = -\log\left(\frac{K_1 \cdot C(CO_2)}{C(HCO_3)}\right) \qquad (24)$$

where K_1 is the first dissociation constant of carbonic acid with a value of 1.3×10^{-6} mol dm^{-3} valid for 2°C, 400 bar and 35 ‰ salinity (Millero, 1995). Average global surface temperatures (T) were calculated using normalized pCO_2 values (RCO_2) and considering the increasing luminosity of the aging sun (Berner, 1994):

$$T(t) = \Gamma \cdot \ln(RCO_2) - W_S \cdot \frac{t}{570} + T(q) \qquad (25)$$

where t is age (in My b. p.), $T(q)$ is the average Quaternary temperature (13.5 ± 1.5; Worsley and Kidder, 1991), Γ is a constant relating pCO_2 and surface temperature and W_S defines the impact of insolation on surface temperature (Berner, 1994). High-resolution models indicate that the sensitivity of surface temperature to pCO_2 and solar luminosity were overestimated in previous simulations (Kothavala et al., 1999; 2000). Moreover, the relation between T and pCO_2 is affected by paleogeography and the presence of large continental ice shields.

Following the approach of the new GECARB III model (Berner and Kothavala, 2001), I used a diminished W_S value (7.4°C) throughout the whole model period, $\Gamma = 3.3$°C for the warm Cretaceous to early Cenozoic and $\Gamma = 4.0$°C for the cold last 40 My.

ModelMaker, Version 3 (Cherwell Scientific Publishing Limited) was used to implement the box model. ModelMaker solves the set of coupled first order differential equations defined in Table 4 using the Runge-Kutta method (Press et al., 1992). Initial values were assigned to each model compartment to define the conditions at the beginning of the Cretaceous ($t =$ 145 My b. p.). Subsequently, the model was integrated forwardly to simulate the changing composition of oceans and atmosphere till the end of the Quaternary ($t = 0$ My b. p.). The initial concentration of Ca was set to a value of 20 mM, two times higher than the current concentration, because Sr/Ca and Mg/Ca ratios in marine carbonates (Renard, 1986) as well as model studies (Hardie, 1996) suggest a high Ca concentration during the early Cretaceous. The initial RCO_2 was set to 3 as suggested by proxy data (Freeman and Hayes, 1992) and previous models (Berner, 1994). Initial concentrations of HCO_3 and CO_2 were calculated from the corresponding pCO_2 and Ca values assuming thermodynamic equilibrium whereas early Cretaceous Sr, $\delta^{13}C$ and $^{87}Sr/^{86}Sr$ values were defined by geological data (Delaney and Boyle, 1986; Hayes et al., 1999; Veizer et al., 1999). The time scale used in the model corresponds to the geological time scale of Harland et al. (1990) because most of the external variables (f_{PB}, f_{IP}, f_{VO}, f_{ER}) and the controlling isotope data ($\delta^{13}C$, $^{87}Sr/^{86}Sr$) refer to this scale (Larson, 1991a; 1991b; Veizer et al., 1999). Mass balance calculations used as a control to the model results showed that masses were completely conserved during numerical integration. A typical model run was completed within 1 min on a PC with Pentium III processor.

3. MODEL RESULTS AND IMPLICATIONS

Presentation of model results starts with the construction of a standard case showing the best agreement between simulation results and independent observations. Based on this reference, different model parameters and process parameterizations are varied to identify key processes controlling the evolution of seawater composition, atmospheric pCO_2 values and global climate.

3.1. The standard case

Seawater concentrations, partial pressures and isotopic ratios produced as output of the model were fitted to independent data by tuning of model parameters. Non-linear optimization procedures implemented in the ModelMaker software (Marquardt method; Press et al., 1992) were applied to minimize deviations between model predictions and observations using the χ^2 merit function. The set of parameter values producing the best fit to the data was defined as standard case. Concentrations of HCO_3, Ca and Sr, partial pressure of CO_2, and carbon masses on continental and oceanic crust predicted for the Quaternary ($t = 0$) were compared to the well-known present values whereas secular trends in Sr/Ca, $^{87}Sr/^{86}Sr$ and $\delta^{13}C$ were related to the continuous record in marine carbonates (Fig. 5).

The procedure started with the optimization of parameter values that define the poorly constrained basalt-seawater interactions at the deep-sea floor ($F_{ALT}(q)$, r_{ALT}, $F^{Sr}_{HY}(q)$, $F^{Sr}_{A}(q)$) using recent seawater concentrations of Ca and HCO_3 (10.4 mM and 2.3 mM, respectively) and the secular trend in marine Sr/Ca ratios (Fig. 5a). Parameters defining the metamorphic release of CO_2 from carbonates on continental and oceanic crust (k_{MC}, r_S) and the weathering of young volcanic rocks (r_{VO}) were optimized using the Quaternary pCO_2 (230 μatm), the amount of pelagic $CaCO_3$ ($1.2 \times 10^{+21}$ mol; Hay et al., 1988; Staudigel et al., 1996) and the $^{87}Sr/^{86}Sr$ record in marine carbonates (Fig. 5b). Turnover of particulate organic carbon (parameters k_{WO}, p, and k_{SO}) was constrained using the $\delta^{13}C$ record in marine carbonates (Fig. 5c) and the whole procedure was repeated until the overall χ^2 merit function defining the deviation between the complete set of observations and predictions was at its minimum. As a result of this procedure, Quaternary fluxes were tuned to the values listed in Tables 1 and 2, parameters r_{ALT} and r_{VO} were set to 0.7, the recycling efficiency r_S was adjusted to 0.2, p was tuned to 0.3, and the kinetic constants k_{MC}, k_{WO}, and k_{SO} were set to 2.5×10^{-4} My^{-1}, 5×10^{-3} My^{-1}, and 5×10^{-5} My^{-1}, respectively.

The results of the standard run are depicted in Figures 5–8 and the corresponding Quaternary fluxes are listed in Tables 1 and 2. Simulated Ca concentrations increased during the Cretaceous and decreased during the Cenozoic (Fig. 6a). The Cretaceous increase was caused by enhanced rates of seafloor spreading (Fig. 2) and hydrothermal Ca release (Eqn. 1) whereas the subsequent drop in Ca is related to diminishing spreading and rising weathering rates. Similar changes in seawater Ca were previously calculated by Hardie (1996) whereas Berner et al. (1983) predicted the opposite trends. The output of Berner's BLAG model is affected by an oversimplified treatment of silicate weathering. The BLAG model considers only weathering of Ca- and Mg-silicates whereas the model presented in this paper considers the weathering of all silicate rocks (including Na- und K-bearing silicates) resulting in a considerably larger and more realistic ratio of HCO_3 to Ca fluxes. Carbonate alkalinity (HCO_3) is related to the inverse Ca concentration (Eqn. 9) so that HCO_3 is depleted in Ca-rich seawater and vice versa (Fig. 6b). In general agreement with previous attempts (Berner, 1991; 1994; Berner et al., 1983; Goddéris and François, 1995; Tajika, 1998), the model calculates high pCO_2 values for the mid-Cretaceous and a continuous pCO_2 decrease throughout the late Cretaceous and Cenozoic (Fig. 6c). Predicted pH values, calculated from HCO_3 and CO_2 concentrations (Eqn. 24), were constantly low during the Cretaceous and early Cenozoic and increased during the late Cenozoic (Fig. 6d). Paleo-pH has been reconstructed using stable boron isotope ratios in planktonic foraminifers assuming constant $^{11}B/^{10}B$ ratios in seawater (Pearson and Palmer, 2000; Spivack et al., 1993). The validity of boron-based paleo-pH values was recently questioned by Lemarchand et al. (2000) who demonstrated that $\delta^{11}B$ in seawater has changed considerably over the Cretaceous and Cenozoic. Nevertheless, the data suggest a pH decrease over the Cenozoic similar to the model curve (Fig. 6d).

Sr/Ca ratios in pelagic carbonates show a regular increase over the Cretaceous and Cenozoic (Delaney and Boyle, 1986; Renard, 1986) which is reproduced by the model (Fig. 5a). The

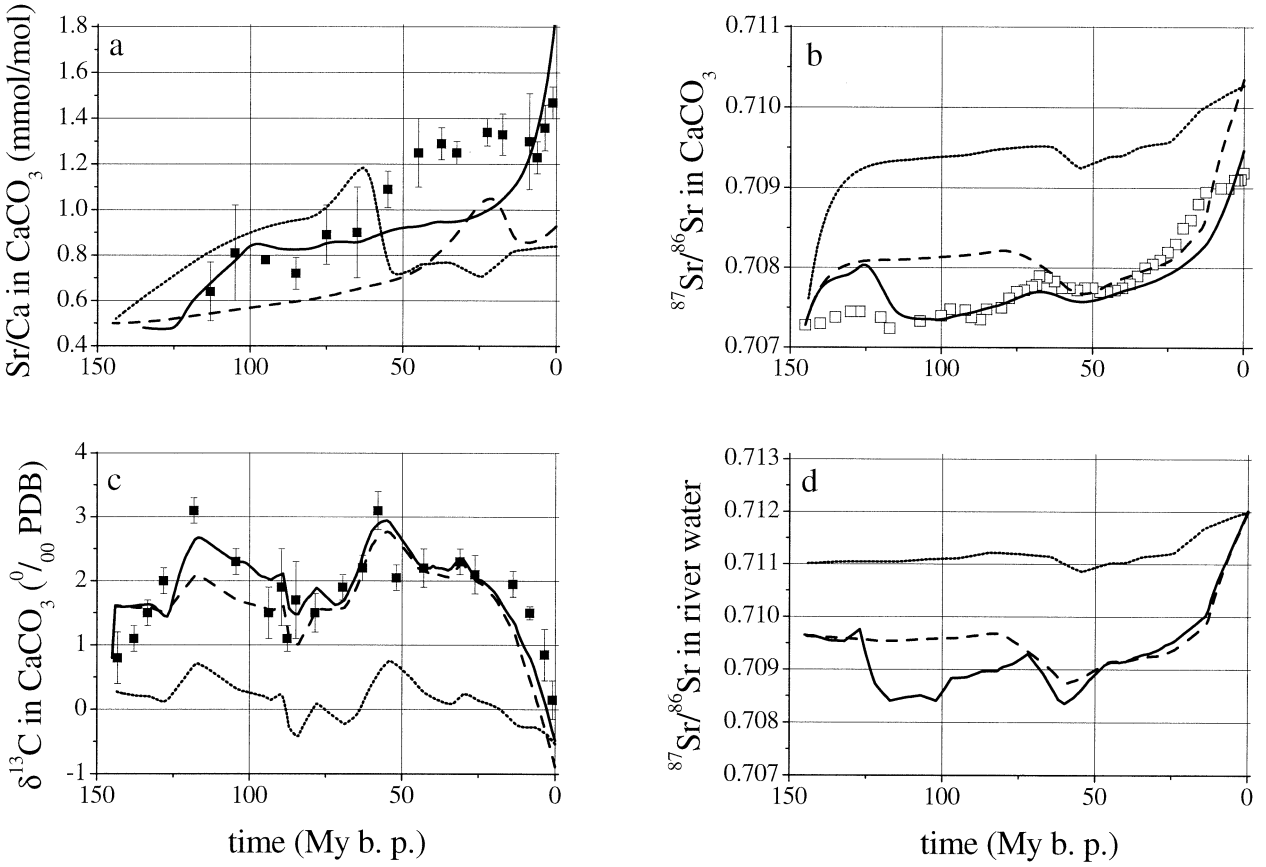

Fig. 5. Element and isotope ratios in marine carbonates and river water. Results of the standard run (solid line), for constant volcanic activity (broken line, $f_{PB} = f_{IP} = f_{VO} = 1$) and for both constant erosion and volcanic activity (dotted line, $f_{PB} = f_{IP} = f_{VO} = f_{ER} = 1$) are compared to data measured in biogenic carbonates. (a) Sr/Ca ratios in marine carbonates calculated with the model and determined by Delaney and Boyle (1986) in planktonic foraminiferal shells (solid squares with vertical error bars). (b) $^{87}Sr/^{86}Sr$ ratios in marine carbonates and seawater. Model results are compared to the isotopic composition of marine carbonate fossils (open squares) reported by Veizer et al., (1999). (c) $\delta^{13}C$ values in marine carbonates and seawater. Model results are compared to the isotopic composition of marine carbonate fossils (solid squares with vertical error bars) reported by Hayes et al. (1999). (d) Isotopic composition of riverine Sr calculated with the model.

fit to the $^{87}Sr/^{86}Sr$ record (Fig. 5b) and marine $\delta^{13}C$ values (Fig. 5c) is also satisfactory implying that the parameterization of carbon, calcium and strontium cycling is appropriate. The $^{87}Sr/^{86}Sr$ ratio in river water defined by the weathering of silicate and carbonate rocks was low during the Cretaceous and increased during the late Cenozoic (Fig. 5d) due to the enhanced weathering of crystalline and sedimentary rocks and an increasingly radiogenic signature of these rocks (section 2. 10) as previously suggested by independent modeling of strontium and carbon isotope data (François and Goddéris, 1998; Goddéris and François, 1996). The low riverine $^{87}Sr/^{86}Sr$ ratio during the Cretaceous clearly shows that the secular trend in marine isotope values not only reflects the changing intensity of submarine volcanism at spreading centers but also the contribution of subaerial volcanic deposits to continental silicate weathering (see also Kump and Arthur, 1997).

Silicate weathering rates are influenced by volcanic and metamorphic CO_2 inputs (Figs. 7a, 9a, 10a). During the mid-Cretaceous, rates were enhanced due to strong mantle degassing whereas the late Cenozoic increase has been induced by metamorphic decomposition of subducted carbonates. Moreover, they are modulated by the weatherability of silicate rocks which is defined here as ratio of weathering rate and feed-back variable $f_B(CO_2)$. It has been high during the mid-Cretaceous and late Cenozoic due to the formation of volcanic deposits and the erosion of crystalline and sedimentary silicate rocks, respectively (Fig. 7b). Weathering of carbonates is influenced by volcanic and metamorphic CO_2 production, exposure of carbonate rocks and weatherability of silicate rocks (Fig. 7c). The weathering of carbonates was at its peak during the early Cenozoic due to the exposure of large continental areas covered with carbonate rocks (variable f_{LA}; Bluth and Kump, 1991) and a rather low weatherability of silicate rocks. Burial of carbonates is mainly determined by carbonate weathering because the dominant portions of Ca and HCO_3 in seawater originate from weathering carbonate rocks (Tables 1 and 2). Thus, the carbonate burial and weathering curves look similar (Fig. 7c and 7d) indicating also that the net effect of carbonate turnover on pCO_2 and ocean chemistry is small. The fit of the predicted burial rates to independently reconstructed accumulation rates (Hay, 1998) is dissatisfactory (Fig. 7d). This mismatch could either be due to a poor presentation of carbonate weathering

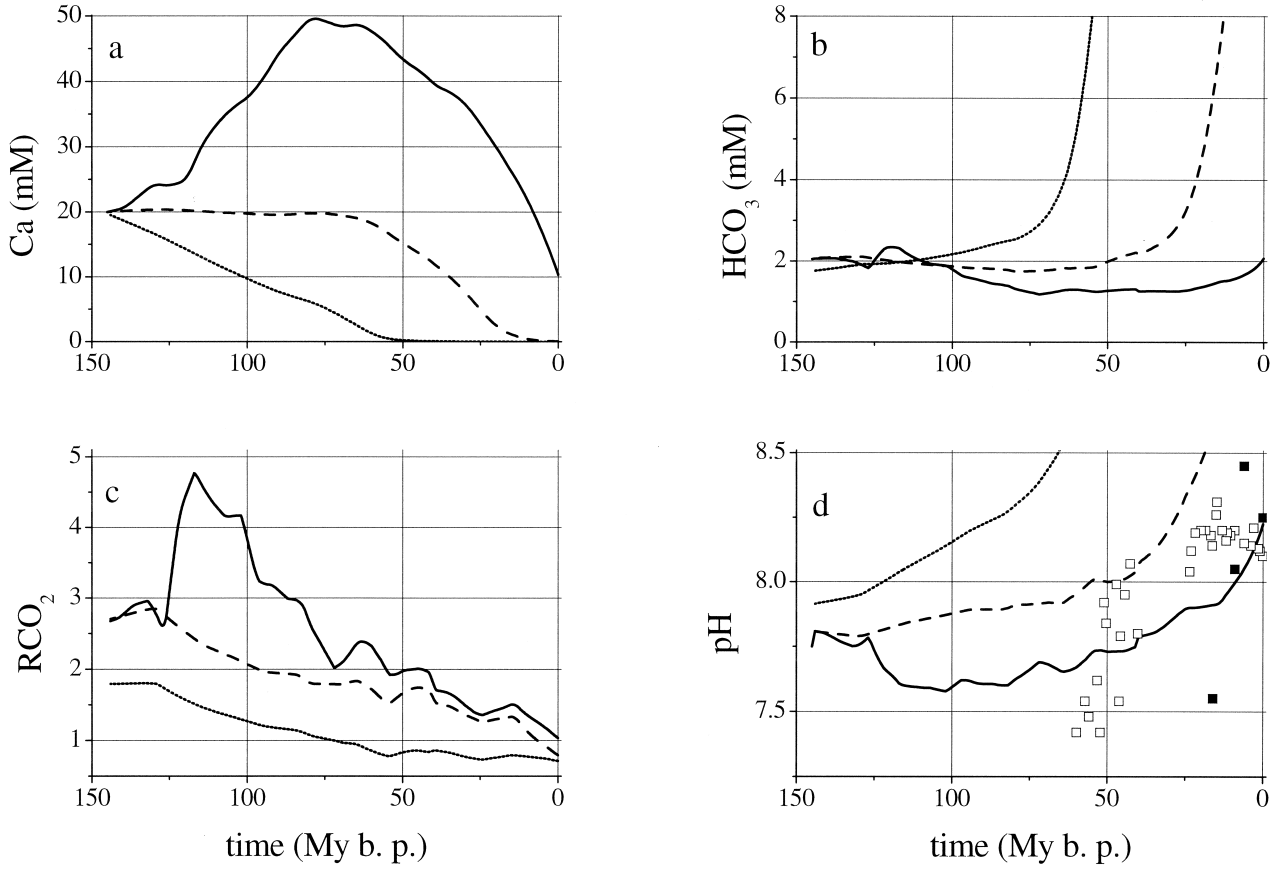

Fig. 6. Seawater and atmosphere composition calculated for the standard case (solid line), for constant volcanic activity (broken line, $f_{PB} = f_{IP} = f_{VO} = 1$) and for both constant erosion and volcanic activity (dotted line, $f_{PB} = f_{IP} = f_{VO} = f_{ER} = 1$). (a) Calcium concentration in seawater; (b) Bicarbonate concentration in seawater; (c) Partial pressure of CO_2 normalized to the Quaternary value (230 μatm); (d) pH value in seawater. Model-pH is compared to paleo-pH in surface waters as calculated from boron isotope ratios in planktonic foraminifer shells by Pearson and Palmer (2000) (open squares) and Spivack et al. (1993) (closed squares).

and/or accumulation in the model or could reflect an erroneous reconstruction of carbonate sedimentation which relies on several questionable assumptions (Mackenzie and Morse, 1992). POC weathering strongly increases during the late Cenozoic (Fig. 7e) due to enhanced erosion and enlarged land area (Eqn. 14). POC accumulation reflects total weathering rates (Eqn. 15) with high values during the mid-Cretaceous and late Cenozoic (Fig. 7f). Over the Cretaceous and early Cenozoic, the POC turnover was dominated by net accumulation; only during the late Cenozoic, weathering approaches accumulation (Fig. 7e, f) due to enhanced erosion (Fig. 3) inducing a strong decrease in marine $\delta^{13}C$ (Fig. 5c). Phosphate accumulation rates were reconstructed by Föllmi (1995; 1996) as a proxy for POC accumulation using ODP sediment data (Fig. 7f). Cenozoic maxima observed in these data also occur in the model curve implying that the POC accumulation is indeed influenced by chemical weathering as postulated by Föllmi (1995; 1996) and confirmed in the model.

Carbon masses bound in sediments and in the mantle changed considerably in the standard simulation (Fig. 8). The POC pool increased continuously because the burial rate surpassed the weathering rate and the rate of metamorphism throughout the model period. Carbonate deposited on continental crust decreased slowly during the Cretaceous and more rapidly during the Cenozoic because the locus of carbonate deposition was shifted from the continents to the deep-sea (variable f_{BCC}, Fig. 4). Consequently, the carbonate masses on oceanic crust increased during the Cenozoic. Carbon in the mantle was stable during the Cretaceous because mantle degassing was compensated by subduction but increased during the late Cenozoic due to enhanced subduction of pelagic carbonates.

Quaternary fluxes calculated for the standard run indicate a balanced carbon cycle (Table 1) and suggest a significant deviation from steady state for the marine Ca and Sr cycles (Table 2). The removal fluxes of Ca and Sr from seawater are larger than the corresponding input fluxes inducing a decrease in seawater concentrations of both Ca and Sr. This imbalance is mainly due to an increase in silicate weathering during the late Cenozoic enhancing the input of HCO_3 and the removal of Ca and Sr via carbonate precipitation.

3.2. Evolution of pCO_2 controlled by volcanic/tectonic activity and erosion

The influence of volcanic and tectonic activity on the geochemical evolution of ocean and atmosphere was tested by

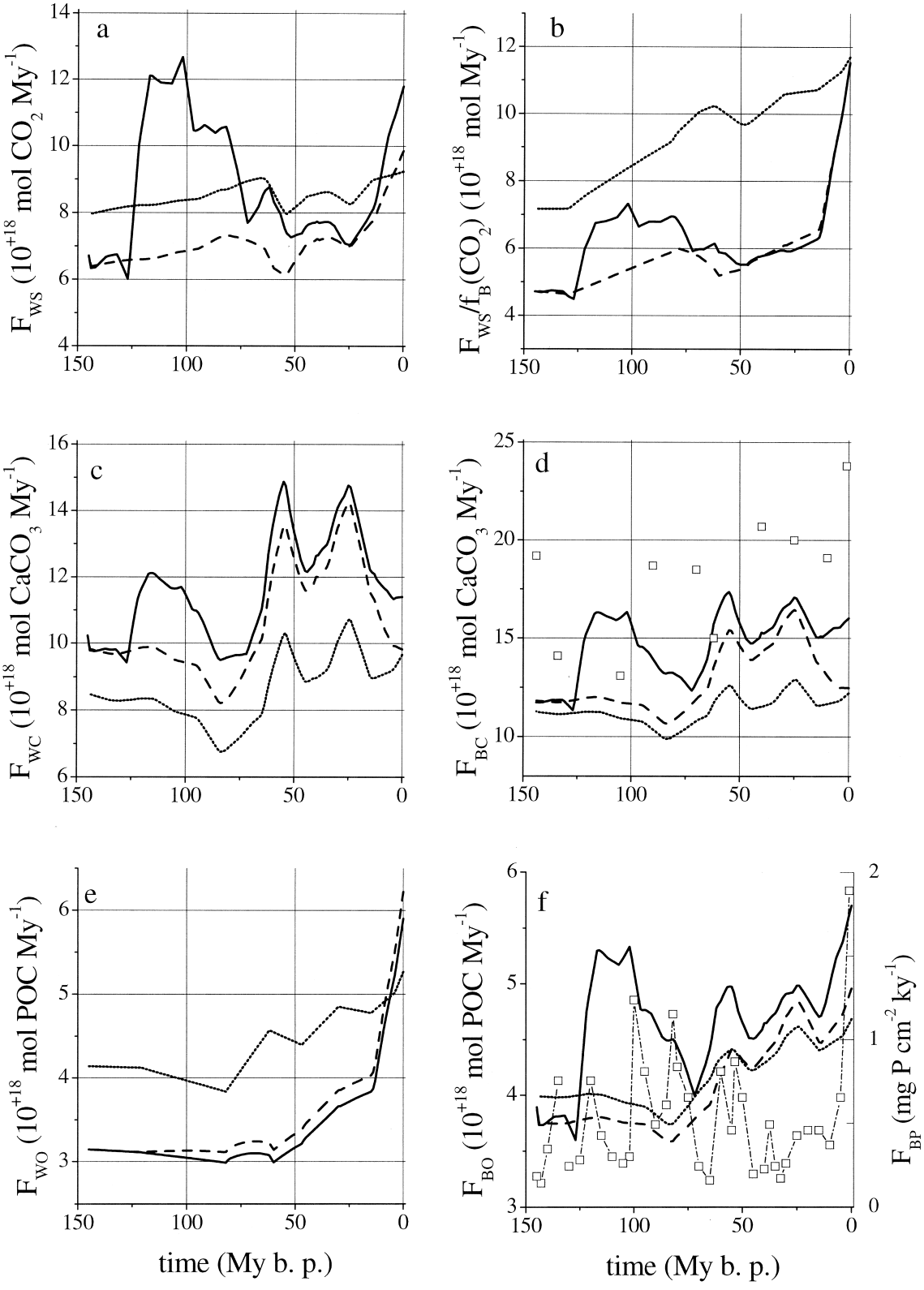

Fig. 7. Fluxes calculated for the standard run (solid line), for constant volcanic activity (broken line, $f_{PB} = f_{IP} = f_{VO} = 1$) and for both constant erosion and volcanic activity (dotted line, $f_{PB} = f_{IP} = f_{VO} = f_{ER} = 1$). (a) Silicate weathering rates; (b) Silicate weatherability (ratio of silicate weathering rate and feed-back variable $f_B(CO_2)$). (c) Carbonate weathering rates; (d) Carbonate burial rates; accumulation rates reconstructed from the sedimentary record (Hay, 1998) are plotted as open squares. e. POC weathering rates. f. POC burial rates (F_{BO}) and phosphate accumulation rates (F_{BP}, open squares with dotted line) independently reconstructed by Föllmi (1996).

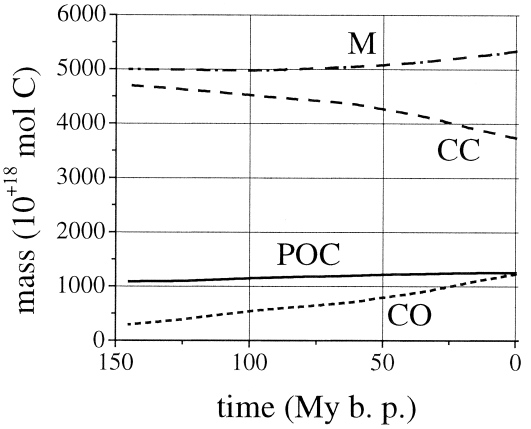

Fig. 8. Carbon masses in model reservoirs calculated for the standard case. Model boxes include particulate organic carbon on continental and oceanic crust (POC), carbonates on continental crust (CC), pelagic carbonates and carbonates in altered oceanic crust (CO), and carbon in the mantle (M).

setting the spreading/subduction rates and the activity of intraplate volcanism to the recent value throughout the model period ($f_{PB} = f_{IP} = f_{VO} = 1$). This operation had a profound impact on the Cretaceous carbon and strontium cycling (Figs. 5 to 7). Silicate weathering was diminished because the change in volcanic activity reduced both CO_2 inputs and silicate weatherability (Fig. 7a, b); seawater Ca was lowered due to the abated hydrothermal fluxes (Fig. 6a); Sr/Ca ratios decreased and $^{87}Sr/^{86}Sr$ ratios increased because of the reduced input of basaltic Sr from midocean ridges and diminished weathering of subaerial volcanic deposits (Fig. 5a, b). Cretaceous $\delta^{13}C$ values decreased (Fig. 5c) due to the lowering of POC burial (Fig. 7f) and pCO_2 values were significantly reduced by the slow-down of mantle degassing (Fig. 6c).

The impact of erosion was analyzed by setting the corresponding variable to the extremely high Quaternary value ($f_{ER} = 1$) for the whole model period whereas the volcanic/tectonic activity was maintained at the low level used in the previous simulation ($f_{PB} = f_{IP} = f_{VO} = 1$). This manipulation produced a strong increase in weatherability of silicate rocks (Fig. 7b), an increase in silicate and POC weathering (Fig. 7a, e) and a corresponding decrease in carbonate turnover (Fig. 7c, d). Changes in silicate and carbonate weathering caused a strong increase in both riverine and marine $^{87}Sr/^{86}Sr$ ratios (Fig. 5b, d) whereas enhanced weatherability of silicate rocks induced a further decrease in pCO_2 (Fig. 6c). The residual decrease in pCO_2 observed at constant volcanic/tectonic activity and erosion was caused by the rise of angiosperms and the marine regression both enhancing weathering rates.

These sensitive tests clearly demonstrate that the simulated evolution of pCO_2 values is mainly controlled via volcanic/tectonic activity and erosion. The formation of a Cretaceous greenhouse by enhanced volcanic activity was postulated previously (Fischer, 1981; Larson, 1991a) and simulated in various box models (Berner, 1991; 1994; Berner et al., 1983; Tajika, 1998). The paramount importance of erosion on the evolution of Cenozoic pCO_2 values is clearly seen in Figure 6c where pCO_2 changes are almost eliminated at constant f_{ER} values. Cenozoic erosion has been accelerated by mountain-

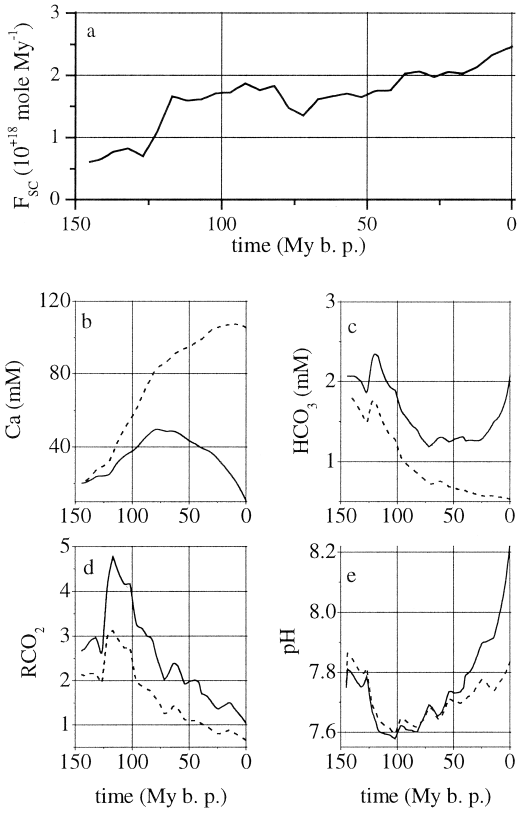

Fig. 9. Effects of metamorphic CO_2 release in subduction zones on the composition of seawater and atmosphere. Results of the standard case (solid line) are compared to a simulation without $CaCO_3$ recycling ($F_{SC} = r_S = 0$, broken line). (a) Release of CO_2 from subducted $CaCO_3$ in the standard case (F_{SC}). (b) Calcium concentration in seawater. (c) Bicarbonate concentration in seawater. (d) Partial pressure of CO_2 normalized to the Quaternary value (230 μatm) (e) pH value in seawater.

building in the Himalayan-Tibetan Plateau region, in the Andes highlands and in western North-America (Raymo, 1989; Raymo and Ruddiman, 1992; Raymo et al., 1988) as well as by the formation of continental ice sheets and glaciers at high latitudes and elevations (Molnar and England, 1990). The model confirms that the development of low pCO_2 levels and ice-house conditions during the late Cenozoic was caused by enhanced erosion and mountain building (Chamberlin, 1899; François and Goddéris, 1998; Goddéris and François, 1995; Raymo, 1989; Raymo and Ruddiman, 1992; Raymo et al., 1988).

3.3. Late Cenozoic evolution of seawater composition affected by $CaCO_3$ turnover in subduction zones

Cenozoic changes in pH, Ca, and HCO_3 concentration were not suppressed at constant volcanic/tectonic activity and erosion (Fig. 6). Thus, the strong Ca decrease and pH increase over the late Cenozoic has been caused by other processes. Here, the key role is taken by CO_2 released at subduction zone volcanoes (Fig. 9a). A complete shut-down of metamorphic CO_2 release at arc volcanoes reduces pCO_2, HCO_3 and Cenozoic pH significantly and strongly enhances Ca concentrations (Fig. 9).

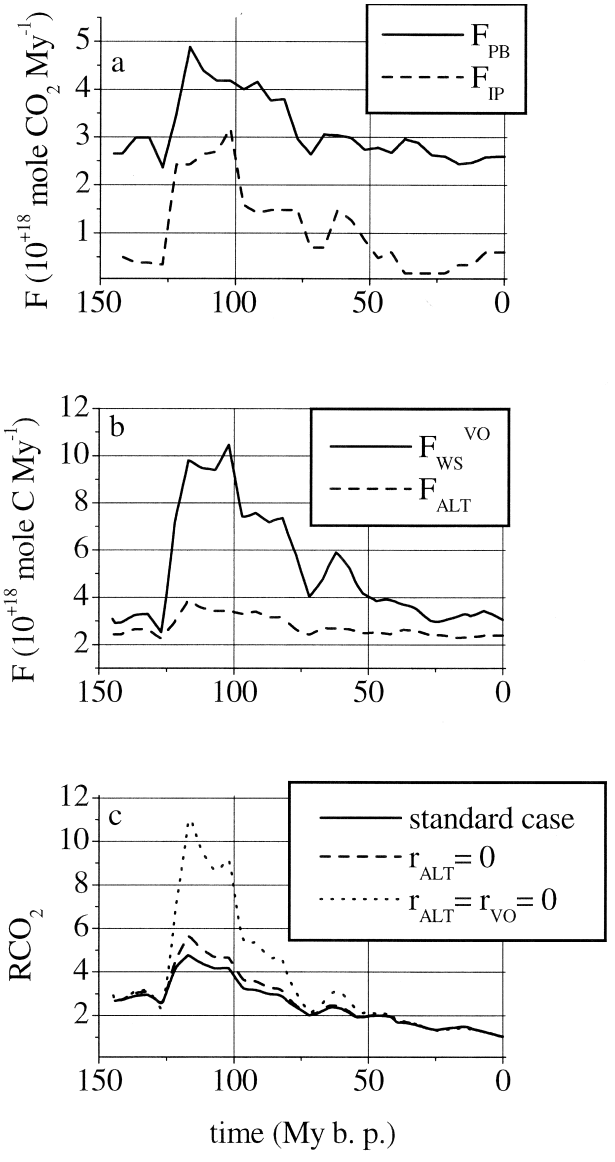

Fig. 10. Effects of volcanic compensation on atmospheric pCO_2. (a) Volcanic CO_2 release via mantle degassing at active plate margins (F_{PB}) and intraplate volcanoes (F_{IP}) in the standard case. (b) CO_2 consumption via weathering of subaerial volcanic deposits (F_{WS}^{VO}) and HCO_3 fixation in altered oceanic crust (F_{ALT}) in the standard case. (c) Normalized partial pressure of CO_2 with variable coupling between volcanic CO_2 emissions and volcanic CO_2 consumption caused by crust alteration and subaerial weathering of volcanic deposits. The standard case with $r_{ALT} = r_{VO} = 0.7$ (solid line) is compared to a model run with decoupled crust alteration ($r_{ALT} = 0$, dashed line) and an other run with both decoupled alteration and weathering ($r_{ALT} = r_{VO} = 0$, dotted line).

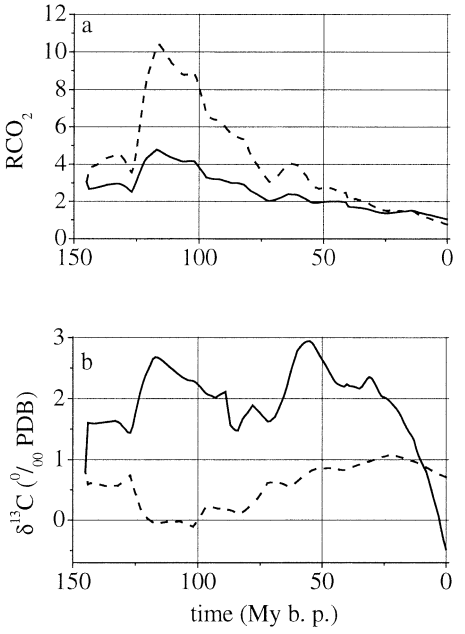

Fig. 11. Effects of POC on atmospheric pCO_2 and marine $\delta^{13}C$ values. The standard case (solid line) is compared to a simulation without POC cycling ($F_{WO} = F_{BO} = F_{SO} = 0$, broken line). (a) Normalized partial pressures of CO_2 (RCO_2). (b) Marine $\delta^{13}C$.

These changes are due to the reduced input of carbonate alkalinity from weathering which is in turn caused by reduced metamorphic CO_2 inputs. In contrast to CO_2 release at spreading centers, CO_2 emissions at arc volcanoes are not accompanied by hydrothermal Ca inputs so that the production of carbonate alkalinity via weathering is not compensated by a corresponding Ca release. Thus, recycling of $CaCO_3$ at arc volcanoes does not only affect the Cenozoic pCO_2 and weathering rates (Caldeira, 1992) but induces also a strong Ca decrease and a significant increase in carbonate alkalinity and seawater pH during the late Cenozoic when pelagic $CaCO_3$ accumulation and metamorphism have been strongly enhanced (Fig. 9).

3.4. Cretaceous pCO_2 level reduced by enhanced burial of organic carbon

Burial of organic carbon acts as efficient CO_2 sink limited by phosphate inputs which are in turn controlled by the intensity of chemical weathering (Eqn. 15; Föllmi, 1995). This relation implies a strong negative feed-back on pCO_2 because weathering and thus POC burial are enhanced under greenhouse conditions. Figure 11a documents that the Cretaceous and early Cenozoic pCO_2 was strongly diminished by the organic carbon cycle whereas the pCO_2 of the latest Cenozoic icehouse has been slightly enhanced by POC turnover. Elimination of the organic subcycle creates a strong minimum in marine $\delta^{13}C$ values during the Cretaceous (Fig. 11b) caused by the emission of mantle-CO_2 with a negative isotopic signature (−5 ‰ PDB) whereas the carbonate data imply a maximum during the Cretaceous (Fig. 5c) which can only be produced by enhanced POC burial. Phosphate cycling and POC burial are also affected by the dissolved oxygen concentrations in bottom water (Colman and Holland, 2000) which is related to the partial pressure of atmospheric O_2 and vertical mixing rates (Van Cappellen and Ingall, 1996). This addition feed-back was not considered in the model. Nevertheless, the good fit to the $\delta^{13}C$ data (Fig. 5c) implies that POC cycling was well represented in the standard case.

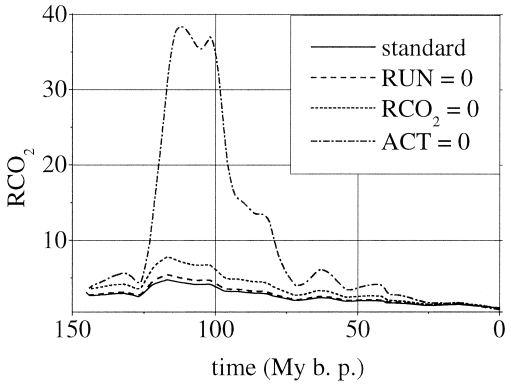

Fig. 12. Impact of the feedback variable $f_B(CO_2)$ on silicate weathering and atmospheric pCO_2. Normalized partial pressures of CO_2 (RCO_2) in the standard case (solid line) are compared to simulations which were run ignoring the effects of temperature-dependent runoff (RUN = 0, dashed line), pCO_2 (RCO_2 = 0, dotted line) and temperature (ACT = 0, dashed - dotted line) on silicate weathering.

3.5. pCO_2 level controlled by temperature-dependence of silicate weathering

The control of silicate weathering via surface temperature exerts a strong stabilizing effect on the pCO_2 level (Walker et al., 1981). Here, and in the GEOCARB models, silicate weathering is controlled by a feedback variable $f_B(CO_2)$ defined as (Berner, 1994; Berner and Kothavala, 2001):

$$f_B(CO_2) = e^{(T(t)-T(q))\cdot ACT} \cdot \left(\frac{2 \cdot RCO_2}{1 + RCO_2}\right)^{0.4} \cdot (1 + RUN \cdot (T(t) - T(q)))^{0.65} \quad (26)$$

where temperature $T(t)$ is calculated from pCO_2 as shown in Eqn. 25. The first exponential term on the right hand site of the equation gives the temperature dependence of silicate weathering, the second term expresses the direct impact of CO_2 on silicate weathering induced by plant fertilization, and the third term defines the influence of temperature-dependent runoff on weathering. The coefficient ACT is related to the activation energy of silicate weathering (ACT = $0.09°C^{-1}$) whereas the coefficient RUN defines the impact of temperature on runoff as determined via general circulation modelling (RUN = $0.025°C^{-1}$ during the Cretaceous and early Cenozoic, RUN = $0.045°C^{-1}$ during the last 40 My).

The effects of runoff, pCO_2, and temperature on silicate weathering and atmospheric pCO_2 were investigated in a series of model runs (Fig. 12). Elimination of the runoff term (RUN = 0) produced only a small change in Cretaceous pCO_2 indicating that an increase in runoff due to elevated temperature had no major effect on pCO_2 and temperature. In contrast, the direct influence of pCO_2 on weathering via plant fertilization is significant as demonstrated by the considerable increase in pCO_2 upon elimination of this feedback (RCO_2 = 0). Finally, the temperature dependence of weathering is clearly the major control on pCO_2 because the normalized partial pressure (RCO_2) increased to extremely high levels during the mid-Cretaceous greenhouse period without this important feedback (ACT = 0). Hence, the modelling confirms that Walker's negative feedback is indeed the major control on atmospheric pCO_2 levels during periods of enhanced mantle degassing.

3.6. Volcanic compensation

Volcanic activity acts not only as major CO_2 source but creates also strong CO_2 sinks. Rates of volcanic CO_2 consumption via alteration of oceanic crust and weathering of subaerial volcanic deposits are strongly influenced by the prevailing level of volcanic activity because fresh volcanic rocks, glasses and ashes are highly reactive consuming CO_2 soon after their emplacement. Moreover, weathering of volcanic deposits is coupled to pCO_2 due to the CO_2 and temperature dependence of silicate weathering. In the model, the pCO_2 dependence is expressed by the variable $f_B(CO_2)$ and the direct link to volcanic activity is considered using the term $r_{VO}(f_{VO} - 1) + 1$ where f_{VO} expresses the level of volcanic activity that changes through time and r_{VO} defines the intensity of coupling (Eqn. 4). The direct coupling between volcanic CO_2 emission and consumption rates creates a dynamic sink which is called volcanic compensation in the following.

Rates of volcanic CO_2 release (F_{PB}, F_{IP}) and volcanic carbon uptake (F_{WS}^{VO}, F_{ALT}) are tightly coupled over the model period (Fig. 10). Crust alteration (F_{ALT}) removes significant amounts of carbonate alkalinity from the ocean whereas weathering of volcanic deposits (F_{WS}^{VO}) converts CO_2 into carbonate alkalinity which is transferred into the ocean to be fixed in oceanic crust or to be transformed into pelagic $CaCO_3$ and CO_2. Figure 10c shows the impact of volcanic compensation on Cretaceous and Cenozoic pCO_2 levels. Decoupling of crust alteration (r_{ALT} = 0) increases the pCO_2 level during the Cretaceous by ~25% whereas pCO_2 is enhanced by more than a factor of 2 when the weathering of subaerial volcanic deposits is decoupled from volcanic activity (r_{VO} = 0). Cenozoic pCO_2 values are not affected because the volcanic activity has been rather low during this period. Thus, volcanic compensation maintained pCO_2 at a moderate level during the mid-Cretaceous and other greenhouse periods induced by enhanced volcanic activity.

Predicted pCO_2 values strongly depend on the activation energy of silicate weathering used in the modeling. The extreme sensitivity of pCO_2 towards one critical model parameter (ACT, Fig. 12) is a major drawback of carbon modelling and the largest source of error in the reconstruction of ancient pCO_2 levels. Fortunately, the range of predicted pCO_2 values is significantly reduced by consideration of volcanic compensation (Fig. 13). Thus, the reliability of simulated pCO_2 levels is strongly enhanced by the new model presented in this paper.

Previous models of the global carbon cycle considered only the negative feed-back established by the CO_2 and temperature dependence of silicate weathering (Walker et al., 1981) but ignored the direct link between rates of volcanic CO_2 release and consumption suggested by recent field studies (Alt and Teagle, 1999; Louvat and Allègre, 1997; Taylor and Lasaga, 1999) and confirmed in the present model. More field work is needed to better define the degree of coupling between volcanic activity and CO_2 consumption both on the continents and at the deep-sea floor.

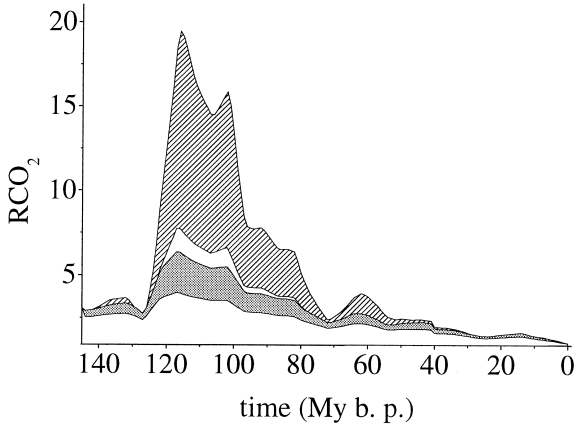

Fig. 13. Range of predicted RCO_2 values. The gray area represents the standard case with variable activation energy for silicate weathering (lower RCO_2 limit: ACT = 0.12°C^{-1}, upper RCO_2 limit ACT = 0.06°C^{-1}). The shaded area was calculated in the absence of volcanic compensation ($r_{ALT} = r_{VO} = 0$) using the same range of activation energies (ACT = 0.06–0.12°C^{-1}).

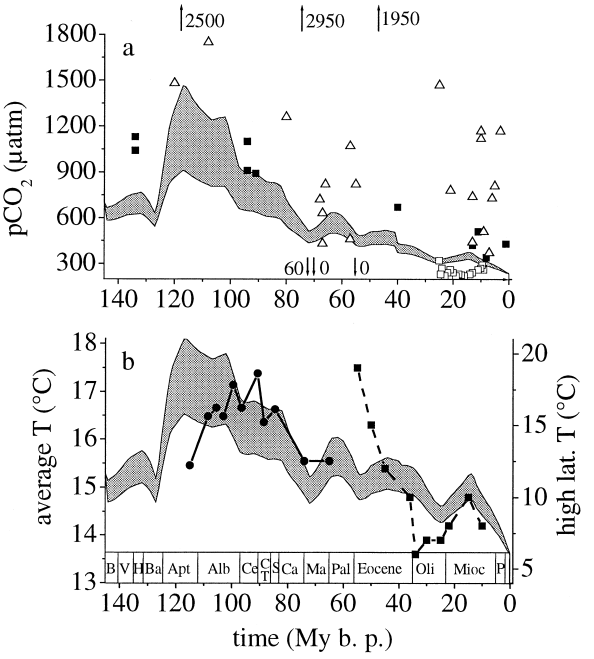

Fig. 14. Cretaceous and Cenozoic evolution of pCO_2 and surface temperature. (a) The gray area indicates the range of pCO_2 produced in the standard run of the model with variable activation energy as defined in Figure 13. Independent paleo-pCO_2 values were derived from $\delta^{13}C$ measurements in sedimentary porphyrins (closed squares; Freeman and Hayes, 1992), alkenones (open squares; Pagani et al., 1999), and paleosol carbonates (open triangles; Ekart et al., 1999). Arrows and numbers indicate paleo-pCO_2 estimates derived from paleosol samples extending beyond the pCO_2 scale. (b) Average global surface temperatures calculated in the standard run (gray area) and surface temperatures at high southern latitudes (~50°S) derived from $\delta^{18}O$ in planktonic foraminiferal $CaCO_3$ (squares; Shackleton and Kennett, 1975) and bulk carbonate (dots; Clarke and Jenkyns, 1999). Epoch boundaries are defined using the time scale of Harland et al. (1990).

3.7. Evolution of pCO_2 and climate during the Cretaceous and Cenozoic

Partial pressures of CO_2 calculated in the standard run of the model show a similar evolution as indicted by independent proxy data (Fig. 14a). They reach a maximum during the mid-Cretaceous, followed by a decrease during the late Cretaceous, an increase towards the early Cenozoic and a further decrease cumulating in the low Quaternary value. The scatter in the proxy data is considerable because the evaluation of $\delta^{13}C$ values in paleosol carbonates and organic molecules relies an a number of assumptions and poorly constrained parameters (Ekart et al., 1999; Freeman and Hayes, 1992; Pagani et al., 1999). Estimates based on foraminiferal $\delta^{11}B$ values were not considered because these data were evaluated assuming constant alkalinity and $\delta^{11}B$ in seawater whereas the model presented in this paper (Fig. 6b) and independent modeling (Lemarchand et al., 2000) demonstrate that seawater composition changed considerably over the model period. Mid-Cretaceous pCO_2 values produced by the model fall into the lower range of proxy data whereas late Cretaceous and Cenozoic model results are not significantly different from the mean proxy values. The mid-Cretaceous maximum of 900 to 1400 μatm produced by the model is consistent with general circulation modeling suggesting a pCO_2 of 1300 to 1400 μatm for this period (Barron et al., 1995).

The Cretaceous was traditionally regarded as the best example of a "greenhouse world" with warm temperatures and reduced equator to pole temperature gradients (Fischer, 1984). Recent studies reveal a more complex picture of the Cretaceous climate evolution (Frakes et al., 1992; Kemper, 1987). Thus, Podlaha et al. (1998) observed a general cooling during the early Cretaceous in northern European fossils and proposed a decrease in sea surface temperatures from ~20°C during the Berrias to ~10°C during the Hauterivian. Extensive deposits of ice-rafted sediments at high latitudes also indicate cool temperatures for the Valanginian and Hauterivian (Frakes et al., 1992). The cool lower Cretaceous with polar ice sheets (Stoll and Schrag, 1996) was followed by a warm mid-Cretaceous with ice-free poles and low latitudinal temperature gradients (Fig. 14b). Paleo data imply a significant warming from the Aptian to Albian, a period of extreme global warmth extending from the Albian to the Santonian followed by a general cooling trend during the Campanian to the Maastrichtian (Clarke and Jenkyns, 1999; Huber, 1998; Huber et al., 1995; Kolodny and Raab, 1988; Veizer et al., 1999). The cooling during the late Cretaceous was followed by a warming during the early Tertiary with a sudden increase in temperature at the Cretaceous/Tertiary boundary (Wolfe, 1990) and a climate optimum during the lower Eocene (Frakes et al., 1992). The subsequent Cenozoic climate evolution is characterized by several cooling steps and increased ice volume since the early Oligocene (Miller et al., 1987). Oxygen isotope data (Fig. 14b) and Mg/Ca ratios indicate rapid cooling episodes at the end of the early Eocene climate optimum, at the base of the Oligocene, during the middle Miocene, and the middle Pliocene (Lear et al., 2000; Shackleton and Kennett, 1975).

Global average surface temperatures calculated from the pCO_2 model curve (Eqn. 25) confirm the independent geological data with a cool early Cretaceous, a strong maximum during the mid-Cretaceous, a continuous cooling towards the

late Cretaceous, a rather warm early Cenozoic and a late-Cenozoic icehouse world (Fig. 14b). Nevertheless, closer inspection of the data reveals deviations between model predictions and independent paleoclimatic data. Thus, the Aptian is the warmest period in the model whereas the geological data suggest the Cenomanian—Santonian as climate optimum. Moreover, the cooling steps that occurred during the early Eocene and Oligocene were not reproduced by the model. It is possible that these deviations are caused by the coarse resolution of the forcing parameters. Thus, erosion rates, which have a paramount influence on simulated pCO_2 values and temperatures, were reconstructed using only two data points for the entire Cretaceous and one value for each Cenozoic epoch. Interestingly, the mid-Miocene climate optimum is well reproduced by the model even though recent proxy data suggest a low pCO_2 (Pagani et al., 1999). Overall, the model did not reveal a significant de-coupling of climate and atmospheric pCO_2 as previously postulated (Flower, 1999) but suggests that the history of climate change has been closely coupled to the evolution of pCO_2 over the Cretaceous and Cenozoic.

4. CONCLUSIONS

Silicate weathering rates are strongly affected by the emplacement of volcanic rocks and deposits. These young and reactive deposits are weathered soon after emplacement providing a dynamic CO_2 sink which effectively stabilizes pCO_2 during periods of enhanced volcanic activity. Young volcanic deposits were the major locus of silicate weathering throughout the Cretaceous and early Cenozoic. Secular trends in marine $^{87}Sr/^{86}Sr$ ratios have been strongly affected by the changing composition of weathering silicates. Low marine $^{87}Sr/^{86}Sr$ values during the Cretaceous not only indicate intense hydrothermal activity at submarine spreading centers but also reflect enhanced weathering of subaerial volcanic deposits.

Production and burial of particulate organic matter are linked to chemical weathering because the limiting nutrient phosphate is released by weathering processes. Due to the temperature- and pCO_2-dependence of weathering, POC burial is enhanced during greenhouse periods producing an additional negative feed-back on pCO_2.

Stabilization of pCO_2 during periods of enhanced volcanic activity is mainly provided by the following mechanisms arranged in order of decreasing efficiency:

$$\begin{array}{c}\text{temperature-dependence}\\ \text{of silicate weathering}\end{array} > \begin{array}{c}\text{weathering of young}\\ \text{volcanic deposits}\end{array} > \begin{array}{c}\text{burial of}\\ \text{POC}\end{array} > \begin{array}{c}CO_2\text{-}\\ \text{fertilization}\end{array}$$

Seawater concentrations of both Ca and Sr changed considerably during the Cretaceous and Cenozoic with an increase during the mid-Cretaceous caused by strong hydrothermal activity and a rapid decrease during the late Cenozoic due to enhanced silicate weathering. Carbonate alkalinity showed the inverse behavior whereas pH increased strongly during the late Cenozoic due to an increase in carbonate alkalinity and a decrease in pCO_2. Changes in seawater Ca, Sr, and HCO_3 should be considered in the evaluation of secular trends observed in marine carbonates ($^{87}Sr/^{86}Sr$, element/Ca ratios, stable B and Ca isotopes).

Subduction zones play a key role in the global carbon cycle. Here, the carbon reservoir in the mantle is replenished with subducted carbonates and POC, CO_2 is released into the atmosphere by the metamorphic decomposition of carbonates and CO_2 is converted into HCO_3^- via weathering of young volcanic deposits. The release of CO_2 at volcanic arcs and enhanced weathering induced a significant increase in carbonate alkalinity and decrease in seawater Ca during the late Cenozoic when pelagic $CaCO_3$ accumulation and metamorphism have been strongly increased.

Evolution of atmospheric pCO_2 during the Cretaceous and Cenozoic can be understood as a consequence of tectonic processes. The mid-Cretaceous greenhouse with pCO_2 values in the range of 900 to 1400 μatm was caused by increased rates of seafloor spreading, subduction, and intraplate volcanisms whereas the pCO_2 decrease during the late Cenozoic has been induced by mountain-building which enhanced erosion and thus silicate weathering rates.

The long-term evolution of average global surface temperatures is mainly driven by changes in atmospheric pCO_2. Thus, the climate optima during the mid-Cretaceous and early Cenozoic are correlated with high pCO_2 values whereas the cool periods during the late Cretaceous and Cenozoic are characterized by low pCO_2 levels.

Acknowledgments—The author would like to thank E. Suess, J. Veizer, H.-U. Schmincke, W. W. Hay, W. Kuhnt, and R. A. Berner for stimulating discussions. The constructive reviews of R. A. Berner and L. M. Francois and the helpful comments of the associated editor L. R. Kump are gratefully acknowledged. This work is contribution No. 2 of the Sonderforschungsbereich 574 "Volatiles and Fluids in Subduction Zones" at Kiel University.

Associate editor: L.R. Kump

REFERENCES

Aiuppa A., Allard P., D'Alessandro W., Michel A., Parello F., Treuil M., and Valenza M. (2000). Mobility and fluxes of major, minor and trace metals during basalt weathering and groundwater transport at Mt. Etna volcano (Sicily). *Geochim. Cosmochim. Acta* **64,** 1827–1841.

Allard P. (1992) Global emissions of helium-3 by subaereal volcanism. *Geophys. Res. Lett.* **19,** 1479–1481.

Alt J. C. and Teagle D. A. H. (1999) The uptake of carbon during alteration of oceanic crust. *Geochim. Cosmochim. Acta* **63,** 1527–1536.

Archer D. (1996a) A data-driven model of the global calcite lysocline. *Glob Biogeochem. Cycl.* **10,** 511–526.

Archer D. E. (1996b) An atlas of the distribution of calcium carbonate in sediments of the deep sea. *Global Biogeochem. Cy.* **10,** 159–174.

Barron E. J., Fawcett P. J., Peterson W. H., Pollard D., and Thompson S. L. (1995) A "simulation" of mid-Cretaceous climate. *Paleoceanography.* **10,** 5953–962.

Berner E. K. and Berner R. A. (1996) Global Environment: Water, Air and Geochemical Cycles. Prentice Hall.

Berner R. A. (1982) Burial of organic carbon and pyrite sulfur in the modern ocean: Its geochemical and environmental significance. *Am. J. Sci.* **282,** 451–473.

Berner R. A. (1991) A model for atmospheric CO_2 over Phanerozoic time. *Am. J. Sci.* **291,** 339–376.

Berner R. A. (1994) GEOCARB II: A revised model of atmospheric CO_2 over Phanerozoic time. *Am. J. Sci.* **294,** 56–91.

Berner R. A. and Kothavala Z. (2001) GEOCARB III:. A revised

model of atmospheric CO_2 over Phanerozoic time. *Am. J. Sci.* in press.
Berner R. A., Lasaga A. C., and Garrels R. M. (1983) The carbonate-silicate geochemical cycle and its effect on atmospheric carbon dioxide over the past 100 million years. *Am. J. Sci.* **283,** 641–683.
Bluth G. J. S. and Kump L. R. (1991) Phanerozoic paleogeology. *Am. J. Sci.* **291,** 284–308.
Broecker W. S. (1982) Ocean chemistry during glacial time. *Geochim. Cosmochim. Acta* **46,** 1689–1705.
Broecker W. S. and Peng T.-H. (1982) *Tracers in the Sea*. Lamont-Doherty Geological Observatory, Columbia University.
Caldeira K. (1992) Enhanced Cenozoic chemical weathering and the subduction of pelagic carbonate. *Nature* **357,** 578–581.
Chamberlin T. C. (1899). An attempt to frame a working hypothesis of the cause of glacial periods on an atmospheric basis. *J. Geol.* **7,** 545–584., 667–685, 751–787.
Clarke L. J. and Jenkyns H. C. (1999) New oxygen isotope evidence for long-term Cretaceous climatic change in the Southern Hemisphere. *Geology* **27,** 699–702.
Colman A. S. and Holland H. D. (2000). The global diagenetic flux of phosphorus from marine sediments to the oceans: Redox sensitivity and the control of atmospheric oxygen levels. In *Marine Authigenesis: From Global to Microbial*, Vol. 66, Society of Sedimentary Geology.
Delaney M. L. and Boyle E. A. (1986) Lithium in foraminiferal shells: implications for high-temperature hydrothermal circulation fluxes and oceanic crustal generation rates. *Earth Planet. Sci. Lett.* **80,** 91–105.
Edmond J. M. (1992) Himalayan tectonics, weathering processes, and the strontium isotope record in marine limestones. *Science* **258,** 1594–1597.
Edmond J. M., Palmer M. R., Measures C. I., Brown E. T., and Huh Y. (1996) Fluvial geochemistry of the eastern slope of the northeastern Andes and its foredeep in the drainage of the Orinoco in Colombia and Venezuela. *Geochim. Cosmochim. Acta* **60,** 2949–2976.
Ekart D., Cerling T. E., Montanez I. P., and Tabor N. J. (1999) A 400 million year carbon isotope record of pedogenic carbonate: implications for paleoatmospheric carbon dioxide. *Am. J. Sci.* **299,** 905–927.
Emerson S. and Hedges J. I. (1988) Processes controlling the organic carbon content of open ocean sediments. *Paleoceanography* **3,** 621–634.
Engebretson D. C., Kelley K. P., Cashman H. J., and Richards M. A. (1992) 180 Million years of subduction. *GSA Today.* **2,** 93–100.
Fischer A. G. (1981) Climatic oscillations in the biosphere. In *Biotic Crisis in Ecological and Evolutionary Time* (ed. M. H. Nitecki), pp. 103–131. Academic Press.
Fischer A. G. (1984) The two Phanerozoic supercycles. In *Catastrophes and Earth History* (ed. W. A. Berggren and J. A. van Couvering), pp. 129–150. Princeton University Press.
Flower B. P. (1999) Warming without high CO_2? *Nature* **399,** 313–314.
Föllmi K. B. (1995) 160 m. y. record of marine sedimentary phosphorus burial: Coupling of climate and continental weathering under greenhouse and icehouse conditions. *Geology* **23,** 859–862.
Föllmi K. B. (1996) The phosphorus cycle, phosphogenesis and marine phosphate-rich deposits. *Earth Sci. Rev.* **40,** 55–124.
Frakes L. A., Francis J. E., and Syktus J. I. (1992) *Climate Modes of the Phanerozoic*. Cambridge University Press.
François L. M. and Goddéris Y. (1998) Isotopic constraints on the Cenozoic evolution of the carbon cycle. *Chem. Geol.* **145,** 177–212.
Freeman K. H. and Hayes J. M. (1992) Fractionation of carbon isotopes by phytoplankton and estimates of ancient CO_2 levels. *Global Biogeochem. Cy.* **6,** 185–198.
Gaillardet J., Dupré B., and Allègre C. J. (1999a) Geochemistry of large river suspended sediments: Silicate weathering or recycling tracer. *Geochim. Cosmochim. Acta* **63(23/24),** 4037–4051.
Gaillardet J., Dupré B., Louvat P., and Allègre C. J. (1999b) Global silicate weathering and CO_2 consumption rates deduced from the chemistry of large rivers. *Chem. Geol.* **159,** 3–30.
Gibbs M. T. and Kump L. R. (1994) Global chemical erosion during the last glacial maximum and the present: sensitivity to changes in lithology and hydrology. *Paleoceanography* **9,** 529–543.
Goddéris Y. and François L. M. (1995) The Cenozoic evolution of the strontium and carbon cycles: relative importance of continental erosion and mantle exchanges. *Chem. Geol.* **126,** 169–190.
Goddéris Y. and François L. M. (1996) Balancing the Cenozoic carbon and alkalinity cycles: Constraints from isotope records. *Geophys. Res. Lett.* **23(25),** 3743–3746.
Hardie L. A. (1996) Secular variation in seawater chemistry: An explanation for the coupled secular variation in the mineralogies of marine limestones and potash evaporites over the past 600 m. y. *Geology* **24(3),** 279–283.
Harland W. B., Armstrong R. L., Cox A. V., Craig L. E., Smith A. G., and Smith D. G. (1990) *A Geologic Time Scale*. Cambridge University Press.
Hay W. W. (1994) Pleistocene-Holocene Fluxes Are Not the Earth's Norm. In *Material Fluxes on the Surface of the Earth* (ed. W. W. Hay and T. Usselman), pp. 15–27. National Academy Press.
Hay W. W. (1998) Carbonate sedimentation through the late Precambrian and Phanerozoic. *Zbl. Geol. Paläont. Teil I.* **1998(5–6),** 435–445.
Hay W. W., Sloan J. L., and Wold C. N. (1988) Mass/age distribution and composition of sediments on the ocean floor and the global rate of sediment subduction. *J. Geophys. Res.* **93(B12),** 14933–14940.
Hay W. W. and Southam J. R. (1975) Calcareous plankton and loss of CaO from the continents. *Geol. Soc. Am. Abstr. Programs.* **7,** 1105.
Hay W. W. and Southam J. R. (1977) Modulation of marine sedimentation by the continental shelves. In *The Fate of Fossil Fuel CO_2 in the Oceans* (ed. N. R. Andersen and A. Malahoff), pp. 569–604. Plenum Press.
Hayes J. M., Strauss H., and Kaufman A. J. (1999) The abundance of ^{13}C in marine organic matter and isotopic fractionation in the global biogeochemical cycle of carbon during the past 800 Ma. *Chem. Geol.* **161,** 103–125.
Hedges J. I. and Keil R. G. (1995) Sedimentary organic matter preservation: an assessment and speculative synthesis. *Mar. Chem.* **49,** 81–115.
Hoefs J. (1997) *Stable Isotope Geochemistry*. Springer-Verlag.
Holland H. D. (1984) *The Chemical Evolution of the Atmosphere and Oceans*. Princeton University Press.
Huber B. T. (1998) Tropical paradise at the Cretaceous poles. *Science* **282,** 2199–2200.
Huber B. T., Hodell B. T., and Hamilton C. P. (1995) Middle-late Cretaceous climate of the southern latitudes: stable isotope evidence for minimal equator-to-pole thermal gradients. *Geol. Soc. Amer. Bull.* **107,** 1164–1191.
Kemper E. (1987) Das Klima der Kreide-Zeit. *Geologisches Jahrbuch, Reihe-A.* **96,** 5–185.
Kerrick D. M. and Caldeira K. (1998) Metamorphic CO_2 degassing from orogenic belts. *Chem. Geol.* **145,** 213–232.
Kerrick D. M., McKibben M. A., Seward T. M., and Caldeira K. (1995) Convective hydrothermal CO_2 emission from high heat flow regimes. *Chem. Geol.* **121,** 285–293.
Kolodny Y. and Raab M. (1988) Oxygen isotopes in phosphatic fish remains from Israel: Paleothermometry of tropical Cretaceous and tertiary shelf waters. *Palaeogeogr. Palaeocl.* **64,** 59–67.
Kothavala Z., Oglesby R. J., and Saltzman B. (1999) Sensitivity of equilibrium surface temperature of CCM3 to systematic changes in atmospheric CO_2. *Geophys. Res. Lett.* **26,** 209–212.
Kothavala Z., Oglesby R. J., and Saltzman B. (2000). Evaluating the climatic response to changes in CO_2 and solar luminosity. *11th Symposium on Global Change Studies*, 348–351.
Kramer J. R. (1994) Old sediment carbon in global budgets. In *Soil Responses to Climate Change*, Vol. 123 (ed. M. D. A. Rounsevell and P. J. Loveland), pp. 169–183. Springer-Verlag.
Kump L. R. and Alley R. B. (1994) Global Chemical Weathering on Glacial Time Scales. In *Material Fluxes on the Surface of the Earth* (ed. W. W. Hay and T. Usselman), pp. 46–60. National Academy Press.
Kump L. R. and Arthur M. A. (1997) Global Chemical Erosion during the Cenozoic: Weatherability Balances the Budgets. In *Tectonic Uplift and Climate Change* (ed. W. F. Ruddiman), pp. 203–235. Plenum Press.
Larson R. L. (1991a) Geological consequences of superplumes. *Geology* **19,** 963–966.

Larson R. L. (1991b) Latest pulse of Earth: Evidence for a mid-Cretaceous superplume. *Geology* **19,** 547–550.
Lear C. H., Elderfield H., and Wilson P. A. (2000) Cenozoic deep-sea temperatures and global ice volumes from Mg/Ca in benthic foraminiferal calcite. *Science* **287,** 269–272.
Lemarchand D., Gaillardet J., Lewin E., and Allègre C. J. (2000) The influence of rivers on marine boron isotopes and implications for reconstructing past ocean pH. *Nature* **408,** 951–954.
Louvat P. and Allègre C. J. (1997) Present denudation rates on the island of Réunion determined by river geochemistry: Basalt weathering and mass budget between chemical and mechanical erosions. *Geochim. Cosmochim. Acta* **61,** 3645–3669.
Ludwig W., Amiotte-Suchet P., and Probst J.-L. (1999) Enhanced chemical weathering of rocks during the last glacial maximum: a sink for atmospheric CO_2? *Chem. Geol.* **159,** 147–161.
Mackenzie F. T. and Morse J. W. (1992) Sedimentary carbonates through Phanerozoic time. *Geochim. Cosmochim. Acta* **56,** 3281–3295.
Marty B. and Jambon A. (1987) C/^{3}He in volatile fluxes from the solid earth. *Earth Planet. Sci. Lett.* **83,** 16–26.
Marty B. and Tolstikhin I. N. (1998) CO_2 fluxes from mid-ocean ridges, arcs and plumes. *Chem. Geol.* **145,** 233–248.
Michalopoulos P. and Aller R. C. (1995) Rapid clay mineral formation in Amazon delta sediments: reverse weathering and oceanic element cycles. *Science* **270,** 614–616.
Miller K. C., Fairbanks R. G., and Mountain G. S. (1987) Tertiary oxygen isotope synthesis, sea level history, and continental margin erosion. *Paleoceanography* **2,** 1–19.
Millero F. J. (1995) Thermodynamics of the carbon dioxide system in the oceans. *Geochim. Cosmochim. Acta* **59,** 661–677.
Molina J. F. and Poli S. (2000) Carbonate stability and fluid composition in subducted oceanic crust: an experimental study of H_2O-CO_2-bearing basalts. *Earth Planet. Sci. Lett.* **176,** 295–310.
Molnar P. and England P. (1990) Late Cenozoic uplift of mountain ranges and global climate change: chicken or egg. *Nature* **346,** 29–34.
Opdyke B. N. and Walker J. C. G. (1992) Return of the coral reef hypothesis: Basin to shelf partitioning of $CaCO_3$ and its effect on atmospheric CO_2. *Geology* **20,** 733–736.
Opdyke B. N. and Wilkinson B. H. (1988) Surface area control of shallow cratonic to deep marine carbonate accumulation. *Paleoceanography* **3,** 685–703.
Otto-Bliesner B. L. (1995) Continental drift, runoff, and weathering feedbacks: Implications from climate model experiments. *J. Geophys. Res.* **100(D6),** 11537–11548.
Pagani M., Arthur M. A., and Freeman K. H. (1999) Miocene evolution of atmospheric carbon dioxide. *Paleoceanography* **14,** 273–292.
Palmer M. R. and Edmond J. M. (1989) The strontium isotope budget of the modern ocean. *Earth Planet. Sci. Lett.* **92,** 11–26.
Pearson P. N. and Palmer M. R. (2000). Atmospheric carbon dioxide concentrations over the past 60 million years. *Nature* **406,** 695–699.
Petit L. R., Jouzel J., Raynaud D., Barkov N. I., Barnola J.-M., Basile I., Bender M., Chappelaz J., Davis M., Delaygue G., Delmotte M., Kotlyakov V. M., Legrand M., Lipenkov V. Y., Lorius C., Pépin L., Ritz C., Saltzman E., and Stievenard M. (1999) Climate and atmospheric history of the past 420,000 years from the Vostok ice core, Antarctica. *Nature* **399,** 429–436.
Petsch S. T. and Berner R. A. (1998) Coupling the geochemical cycles of C, P, Fe, and S: The effect on atmospheric O_2 and the isotopic records of carbon and sulfur. *Am. J. Sci.* **298,** 246–262.
Plank T. and Langmuir C. H. (1998) The chemical composition of subducting sediment and its consequences for the crust and mantle. *Chem. Geol.* **145,** 325–394.
Podlaha O. G., Mutterlose J., and Veizer J. (1998) Preservation of $\delta^{18}O$ and $\delta^{13}C$ in belemnite rostra from the Jurrasic/Early Cretaceous successions. *Am. J. Sci.* **298,** 324–347.
Press W. H., Teukolsky S. A., Vetterling W. T., and Flannnery B. P. (1992) *Numerical Recipes*. Cambridge University Press.
Raymo M. E. (1989) Geochemical evidence supporting T. C. Chamberlin's theory of glaciation. *Geology* **19,** 344–347.
Raymo M. E. and Ruddiman W. F. (1992) Tectonic forcing of late Cenozoic climate. *Nature* **359,** 117–122.
Raymo M. E., Ruddiman W. F., and Froelich P. N. (1988) Influence of late Cenozoic montain building on ocean geochemical cycles. *Geology* **16,** 649–653.
Rea D. K. and Ruff L. J. (1996) Composition and mass flux of sediment entering the world's subduction zones: Implications for global sediment budgets, great earthquakes, and volcanism. *Earth Planet. Sci. Lett.* **140,** 1–12.
Renard M. (1986) Pelagic carbonate chemostratigraphy (Sr, Mg, ^{18}O, ^{13}C). *Marine Micropaleontology.* **10,** 117–164.
Richter F. M., Rowley D. B., and DePaolo D. J. (1992) Sr isotope evolution of seawater: the role of tectonics. *Earth Planet. Sci. Lett.* **109,** 11–23.
Romanek C. S., Grossman E. L., and Morse J. W. (1992) Carbon isotope fractionation in synthetic aragonite and calcite: Effects of temperature and precipitation rate. *Geochim. Cosmochim. Acta* **56,** 419–430.
Ronov A. B. (1993) Stratisfera - Ili Osadochnaya Obolochka Zemli (Kolichestvennoe Issledovanie) (ed. A. A. Yaroshevskii). Nauka.
Ronov A. B. (1994) Phanerozoic transgressions and regressions on the continents: a quantitative approach based on areas flooded by the sea and areas of marine and continental deposition. *Am. J. Sci.* **294,** 777–801.
Sano Y. and Williams S. N. (1996) Fluxes of mantle and subducted carbon along convergent plate boundaries. *Geophys. Res. Lett.* **23,** 2749–2752.
Sansone F. J., Mottl M. J., Olson E. J., Wheat C. G., and Lilley M. D. (1998) CO_2-depleted fluids from mid-ocean ridge-flank hydrothermal springs. *Geochim. Cosmochim. Acta* **62,** 2247–2252.
Seward T. M. and Kerrick D. M. (1996) Hydrothermal CO_2 emission from the Taupo Volcanic Zone, New Zealand. *Earth Planet. Sci. Lett.* **139,** 105–113.
Shackleton N. J. and Kennett J. P. (1975) Paleotemperature history of the Cenozoic and the initiation of Antarctic glaciation: oxygen and carbon isotope analyses in DSDP sites 277, 279, 281. *Initial Rep. Deep Sea* **29,** 743–755.
Siegenthaler U. and Sarmiento J. L. (1993) Atmospheric carbon dioxide and the ocean. *Nature* **365,** 119–125.
Spivack A. J. and Staudigel H. R. (1994) Low-temperature alteration of the upper oceanic crust and the alkalinity budget of seawater. *Chem. Geol.* **115,** 239–247.
Spivack A. J., You C.-F., and Smith H. L. (1993) Foraminiferal boron isotope ratios as a proxy for surface ocean pH over the past 21 Myr. *Nature* **363,** 149–151.
Staudigel H., Davies G. R., Hart S. R., Marchant K. M., and Smith B. M. (1995) Large scale isotopic Sr, Nd and O isotopic anatomy of altered oceanic crust: DSDP/ODP sites 417/418. *Earth Planet. Sci. Lett.* **130,** 169–185.
Staudigel H., Plank T., White B., and Schmincke H.-U. (1996) Geochemical Fluxes During Seafloor Alteration of the Basaltic Upper Oceanic Crust: DSDP Sites 417 and 418. In *Subduction Top to Bottom*, Vol. 96 (ed. G. E. Bebout, D. W. Scholl, S. H. Kirby, and J. P. Platt), pp. 19–38. AGU.
Staudigel H. R., Hart S. R., Schmincke H. U., and Smith B. M. (1990) Cretaceous ocean crust at DSDP Sites 417 and 418: Carbon uptake from weathering versus loss by magmatic outgassing. *Geochim. Cosmochim. Acta* **53,** 3091–3094.
Stoll H. M. and Schrag D. P. (1996) Evidence for glacial control of rapid sea level changes in the early Cretaceous. *Science* **272,** 1771–1774.
Tajika E. (1998) Climate change during the last 150 million years: reconstruction from a carbon cycle model. *Earth Planet. Sci. Lett.* **160,** 695–707.
Taylor A. S. and Lasaga A. C. (1999) The role of basalt weathering in the Sr isotope budget of the oceans. *Chem. Geol.* **161,** 199–214.
Teagle D. A. H., Alt J. C., Bach W., Halliday A. N., and Erzinger J. (1996) Alteration of upper ocean crust in a ridge-flank hydrothermal upflow zone: Mineral, chemical, and isotopic constraints from hole 896A. *Proceedings of the Ocean Drilling Program, Scientific Results.* **148,** 119–150.
Trull T., Nadeau S., Pineau F., Polvé M., and Javoy M. (1993) C-He systematics in hotspot xenoliths: Implications for mantle carbon contents and carbon recycling. *Earth Planet. Sci. Lett.* **118,** 43–64.
Van Cappellen P. and Ingall E. D. (1996) Redox stabilization of the

atmosphere and oceans by phosphorus-limited marine productivity. *Science* **271,** 493–496.

Veizer J., Ala D., Azmy K., Bruckschen P., Buhl D., Bruhn F., Carden G. A. F., Diener A., Ebneth S., Goddéris Y., Jasper T., Korte C., Pawellek F., Podlaha O. G., and Strauss H. (1999) $^{87}Sr/^{86}Sr$, $\delta^{13}C$, and $\delta^{18}O$ evolution of Phanerozoic seawater. *Chem. Geol.* **161,** 59–88.

Veizer J., Goddéris Y.-F., and François L. M. (2000). Evidence for decoupling of atmospheric CO_2 and global climate during the Phanerozoic eon. *Nature* **408,** 698–701.

Veizer J. and Hoefs J. (1976) The nature of $^{18}O/^{16}O$ and $^{13}C/^{12}C$ secular trends in sedimentary carbonates. *Geochim. Cosmochim. Acta* **40,** 1387–1395.

Veizer J. and Jansen S. L. (1979) Basement and sedimentary recycling and continental evolution. *J. Geol.* **87,** 341–370.

Vitousek P. M., Chadwick O. A., Crews T. E., Fownes J. H., Hendricks D. M., and Herbert D. (1997) Soil and ecosystem development across the Hawaiian Islands. *GSA Today.* **7,** 1–8.

Von Huene R. and Scholl D. W. (1991) Observations at convergent margins concerning sediment subduction, subduction erosion, and the growth of continental crust. *Rev. Geophys.* **29,** 279–316.

Walker J. C. G., Hays P. B., and Kasting J. F. (1981) A negative feedback mechanism for the long-term stabilization of Earth's surface temperature. *J. Geophys. Res.* **86,** 9776–9782.

Wallmann K. (1999) Die Rolle der Subduktionszonen im globalen Wasser- und Kohlenstoffkreislauf. Habilitationsschrift, Christian-Albrechts-Universität.

Wallmann K. (2001). The geological water cycle and the evolution of marine $\delta^{18}O$ values. Geochim. Cosmochim. Acta in press.

Wolfe J. A. (1990) Palaeobotanical evidence for a marked temperature increase following the Cretaceous/Tertiary boundary. *Nature* **343,** 153–156.

Worsley T. R. and Kidder D. L. (1991) First-order coupling of paleogeography and CO_2 with global surface temperature and its latitudinal contrast. *Geology* **19,** 1161–1164.